JOURNAL OF GEOPHYSICAL RESEARCH, VOL. 111, E12S12, doi:10.1029/2006JE002771, 2006

Overview of the Opportunity Mars Exploration Rover Mission to Meridiani Planum: Eagle Crater to Purgatory Ripple

S. W. Squyres,[1] R. E. Arvidson,[2] D. Bollen,[1] J. F. Bell III,[1] J. Brückner,[3] N. A. Cabrol,[4] W. M. Calvin,[5] M. H. Carr,[6] P. R. Christensen,[7] B. C. Clark,[8] L. Crumpler,[9] D. J. Des Marais,[10] C. d'Uston,[11] T. Economou,[12] J. Farmer,[7] W. H. Farrand,[13] W. Folkner,[14] R. Gellert,[15] T. D. Glotch,[14] M. Golombek,[14] S. Gorevan,[16] J. A. Grant,[17] R. Greeley,[7] J. Grotzinger,[18] K. E. Herkenhoff,[19] S. Hviid,[20] J. R. Johnson,[19] G. Klingelhöfer,[21] A. H. Knoll,[22] G. Landis,[23] M. Lemmon,[24] R. Li,[25] M. B. Madsen,[26] M. C. Malin,[27] S. M. McLennan,[28] H. Y. McSween,[29] D. W. Ming,[30] J. Moersch,[29] R. V. Morris,[30] T. Parker,[14] J. W. Rice Jr.,[7] L. Richter,[31] R. Rieder,[3] C. Schröder,[21] M. Sims,[10] M. Smith,[32] P. Smith,[33] L. A. Soderblom,[19] R. Sullivan,[1] N. J. Tosca,[28] H. Wänke,[3] T. Wdowiak,[34] M. Wolff,[35] and A. Yen[14]

Received 9 June 2006; revised 18 September 2006; accepted 10 October 2006; published 15 December 2006.

[1] The Mars Exploration Rover Opportunity touched down at Meridiani Planum in January 2004 and since then has been conducting observations with the Athena science payload. The rover has traversed more than 5 km, carrying out the first outcrop-scale investigation of sedimentary rocks on Mars. The rocks of Meridiani Planum are sandstones formed by eolian and aqueous reworking of sand grains that are composed of mixed fine-grained siliciclastics and sulfates. The siliciclastic fraction was produced by chemical alteration of a precursor basalt. The sulfates are dominantly Mg-sulfates and also include Ca-sulfates and jarosite. The stratigraphic section observed to date is dominated by eolian bedforms, with subaqueous current ripples exposed near the top of the section. After deposition, interaction with groundwater produced a range of diagenetic features, notably the hematite-rich concretions known as ''blueberries.'' The bedrock at Meridiani is highly friable and has undergone substantial erosion by wind-transported basaltic sand. This sand, along with concretions and concretion fragments eroded from the rock, makes up a soil cover that thinly and discontinuously buries the bedrock. The soil

[1]Department of Astronomy, Cornell University, Space Sciences Building, Ithaca, New York, USA.
[2]Department Earth and Planetary Sciences, Washington University, St. Louis, Missouri, USA.
[3]Max Planck Institut für Chemie, Kosmochemie, Mainz, Germany.
[4]NASA Ames/SETI Institute, Moffett Field, California, USA.
[5]Department of Geological Sciences, University of Nevada, Reno, Reno, Nevada, USA.
[6]U.S. Geological Survey, Menlo Park, California, USA.
[7]Department of Geological Sciences, Arizona State University, Tempe, Arizona, USA.
[8]Lockheed Martin Corporation, Littleton, Colorado, USA.
[9]New Mexico Museum of Natural History and Science, Albuquerque, New Mexico, USA.
[10]NASA Ames Research Center, Moffett Field, California, USA.
[11]Centre d'Etude Spatiale des Rayonnements, Toulouse, France.
[12]Enrico Fermi Institute, University of Chicago, Chicago, Illinois, USA.
[13]Space Science Institute, Boulder, Colorado, USA.
[14]Jet Propulsion Laboratory, California Institute of Technology, Pasadena, California, USA.
[15]Department of Physics, University of Guelph, Guelph, Ontario, Canada.
[16]Honeybee Robotics, New York, USA.
[17]Center for Earth and Planetary Studies, Smithsonian Institution, Washington, D. C., USA.
[18]Division of Geological and Planetary Sciences, California Institute of Technology, Pasadena, California, USA.
[19]U.S. Geological Survey, Flagstaff, Arizona, USA.
[20]Max Planck Institut für Sonnensystemforschung, Katlenburg-Lindau, Germany.
[21]Institut für Anorganische und Analytische Chemie, Johannes Gutenberg-Universität, Mainz, Germany.
[22]Botanical Museum, Harvard University, Cambridge, Massachusetts, USA.
[23]NASA Glenn Research Center, Cleveland, Ohio, USA.
[24]Department of Atmospheric Sciences, Texas A&M University, College Station, Texas, USA.
[25]Department of Civil and Environmental Engineering and Geodetic Science, Ohio State University, Columbus, Ohio, USA.
[26]Niels Bohr Institute, Ørsted Laboratory, Copenhagen, Denmark.
[27]Malin Space Science Systems, San Diego, California, USA.
[28]Department of Geosciences, State University of New York, Stony Brook, New York, USA.
[29]Department of Earth and Planetary Sciences, University of Tennessee, Knoxville, Tennessee, USA.
[30]NASA Johnson Space Center, Houston, Texas, USA.
[31]DLR Institute of Space Simulation, Cologne, Germany.
[32]NASA Goddard Space Flight Center, Greenbelt, Maryland, USA.
[33]Lunar and Planetary Laboratory, University of Arizona, Tucson, Arizona, USA.
[34]Department of Physics, University of Alabama at Birmingham, Birmingham, Alabama, USA.
[35]Space Science Institute, Martinez, Georgia, USA.

0148-0227/06/2006JE002771$09.00

surface exhibits both ancient and active wind ripples that record past and present wind directions. Loose rocks on the soil surface are rare and include both impact ejecta and meteorites. While Opportunity's results show that liquid water was once present at Meridiani Planum below and occasionally at the surface, the environmental conditions recorded were dominantly arid, acidic, and oxidizing and would have posed some significant challenges to the origin of life.

Citation: Squyres, S. W., et al. (2006), Overview of the Opportunity Mars Exploration Rover Mission to Meridiani Planum: Eagle Crater to Purgatory Ripple, *J. Geophys. Res.*, *111*, E12S12, doi:10.1029/2006JE002771.

1. Introduction

[2] The Mars Exploration Rover Opportunity landed at Meridiani Planum on Mars on 25 January 2004 at 04:54:22.7 (Earth receive time 05:05:26.6) UTC. The lander came to rest in a small impact crater approximately 20 m in diameter located at 1.9462° south latitude and 354.4734° east longitude, relative to the International Astronomical Union 2000 body-centered coordinate frame [*Squyres et al.*, 2004a, *Arvidson et al.*, 2004]. The primary scientific objective of Opportunity and her sister rover, Spirit, has been to read the geologic record at two landing sites on Mars, and to assess past environmental conditions and their suitability for life. Both rovers are equipped with the Athena science payload [*Squyres et al.*, 2003] (see also Table 1). The investigation has been carried out using rover-acquired remote sensing data to select rock and soil targets, the rover's mobility system to move to those targets, and arm-mounted in situ sensors to investigate targets in detail. Through more than 500 Martian days, or sols, we have used data from Opportunity to investigate the geology, geochemistry and mineralogy of Meridiani Planum, including evidence of past interaction of surface and subsurface water with materials there.

[3] Opportunity's nominal mission, like Spirit's, was planned to last for 90 sols. The initial results of the nominal mission were previously reported by *Squyres et al.* [2004a] and associated papers. In this special section we summarize the major activities and scientific results for the first 511 sols of Opportunity's mission. After landing in Eagle crater, Opportunity spent the first 57 sols exploring rock outcrops exposed in the crater wall, as well as soils on the crater floor. After exiting the crater, Opportunity traveled east to Endurance crater, arriving there on Sol 95 and investigating that crater through Sol 315. Leaving Endurance crater, Opportunity proceeded southward across Meridiani Planum, traversing eolian bedforms and investigating rock and soil targets along the way. As of Sol 511, Opportunity had traversed 5.4 km. (The names used in this paper for landforms, rocks, and other targets were selected by the science team as a convenient way to identify features and targets for which observations were made. All of the impact craters at Opportunity's landing site have been named after historic ships of exploration. None of the feature names in this paper have been approved by the International Astronomical Union.)

[4] This introductory paper is the lead-in to other papers that describe in detail scientific observations and results from the Meridiani landing site. Several papers focus specifically on the results from individual payload elements [*Fergason et al.*, 2006; *Glotch and Bandfield*, 2006; *Johnson et al.*, 2006a; 2006b; *Morris et al.*, 2006; W. H. Farrand et al., Visible and near infrared multispectral analysis of in situ and displaced rocks, Meridiani Planum, Mars by the Mars Exploration Rover Opportunity: Spectral properties and stratigraphy, submitted to *Journal of Geophysical Research*, 2006 (hereinafter referred to as Farrand et al., submitted manuscript, 2006); W. Goetz et al., Overview of the RAT magnet investigation on Spirit and Opportunity, submitted to *Journal of Geophysical Research*, 2006; K. Kinch et al., Radiative transfer analysis of dust deposition on the Mars Exploration Rover Panoramic Camera (Pancam) calibration targets, submitted to *Journal of Geophysical Research*, 2006]. Others present geologic findings from multiple payload elements [*Glotch et al.*, 2006b; *Golombek et al.*, 2006; *Jerolmack et al.*, 2006; *Weitz et al.*, 2006; *Yen et al.*, 2006]. Two papers focus on atmospheric investigations [*Bell et al.*, 2006; *Smith et al.*, 2006]. Three papers describe the results of coordinated experiments with orbiter instruments [*Arvidson et al.*, 2006b; *Wolff et al.*, 2006; J. Griffes et al., Geologic and spectral mapping of etched terrain deposits in northern Meridiani Planum, submitted to *Journal of Geophysical Research*, 2006], and R. Li et al. (Opportunity rover localization and topographic mapping at the landing site of Meridiani Planum, Mars, submitted to *Journal of Geophysical Research*, 2006) report the results of localization studies.

[5] This collection of papers also includes five papers presenting results from the Spirit rover at Gusev crater [*Greeley et al.*, 2006; *Hurowitz et al.*, 2006; *McSween et al.*, 2006; *Ruff et al.*, 2006; B. C. Clark et al., Evidence for montmorillonite or its compositional equivalent in Columbia Hills, Mars, submitted to *Journal of Geophysical Research*, 2006]. For background on Spirit's mission, see *Arvidson et al.* [2006a].

2. Mission Operations

[6] An approach for operating Spirit and Opportunity that translated the mission's scientific objectives into specific rover and payload tasks was defined before landing [*Squyres et al.*, 2003]. In addition, operational testing and rehearsals using the FIDO rover were conducted to develop and refine operational concepts [*Arvidson et al.*, 2002]. More complex operational concepts (for example, acquiring large mosaics with the Microscopic Imager) were developed in response to discoveries made after landing on Mars. The operations approaches used during the mission are described in detail by *Arvidson et al.* [2006a]; a brief summary is provided here.

[7] Each sol (Mars solar day, which is about 24 hours, 39 minutes, 35 seconds long) during Opportunity's mission

Table 1. Athena Payload and Engineering Camera Descriptions

Instrument	Key Parameters
	Mast-Mounted
Pancam: Panoramic Camera	Twelve bands (0.4 to 1.0 μm) for multispectral stereoscopic imaging with 0.28 mrad IFOV; 16.8 deg FOV, 30 cm stereo baseline separation. External calibration target on rover deck.
Mini-TES: Thermal Emission Spectrometer	Emission spectra (5 to 29 μm, 10 cm^{-1} resolution) with 8 or 20 mrad FOV. Internal and external blackbody calibration targets.
	IDD-Mounted in Situ Package
APXS: Alpha Particle X-Ray Spectrometer	^{244}Cm alpha particle sources, α- and X-ray detectors, 3.8 cm FOV.
MB: Mössbauer Spectrometer	^{57}Fe spectrometer in backscatter mode; Co/Rh source and Si-PIN diode detectors; field of view approximately 1.5 cm^2.
MI: Microscopic Imager	30 μm/pixel monochromatic imager (1024 $\times$ 1024) with 6 mm depth of field.
RAT: Rock Abrasion Tool	Tool capable of preparing 5 mm deep by 4.5 cm wide surface on rocks.
	Magnets
Filter	Located front of rover within Pancam FOV. Weak magnet to cull suspended particles from atmosphere.
Capture	Located front of rover within Pancam FOV adjacent to Filter Magnet. Strong magnet to cull suspended particles from atmosphere.
Sweep	Located next to Pancam calibration target. Intended to separate magnetic from nonmagnetic particles. To be examined by Pancam.
RAT	Four magnets of different strengths in RAT. To be examined by Pancam when IDD points RAT toward cameras.
	Engineering Cameras
Navigation Cameras (Navcam)	Mast-mounted panchromatic stereoscopic imaging system with 0.77 mrad IFOV; 45 deg FOV, 20 cm stereo baseline separation. For planning sequences.
Hazard Avoidance Cameras (Hazcam)	Front and rear-looking panchromatic stereoscopic imaging systems with 2 mrad IFOV; 123 deg FOV, 10 cm stereo baseline separation. For path planning and hazard avoidance during traverses.

typically focused on (1) remote sensing of the surface with the Panoramic Camera (Pancam) and/or Miniature Thermal Emission Spectrometer (Mini-TES), (2) a long drive, (3) a short drive to approach a science target with the objective of placing it within the work volume of the Instrument Deployment Device (IDD), or (4) use of the IDD for in situ work involving the Rock Abrasion Tool (RAT) and/or IDD-mounted instruments (Microscopic Imager (MI), Alpha Particle X-Ray Spectrometer (APXS), Mössbauer Spectrometer (MB)). In some instances, more than one class of objectives was addressed on a single sol. For example, a brief "touch and go" measurement with an IDD-mounted instrument like the MI or APXS could precede a drive. Long drives were normally followed immediately by acquisition of partial or full panoramas with the rover's Navigation Cameras (Navcams), often supplemented by Pancam partial stereo panoramas, and all drives were followed by images of the IDD work volume with the Hazard Avoidance Cameras (Hazcams). Every sol normally included routine atmospheric monitoring observations.

[8] A complete investigation of a rock target would include MI imaging and APXS and MB integrations on the rock's surface (the natural surface and/or after brushing with the RAT), abrasion with the RAT to a depth of several mm, repeat MI imaging and APXS and MB integration on the abraded surface, and Mini-TES and 13-filter Pancam observations before and after RAT abrasion. Time constraints, data volume constraints, and/or scientific considerations often dictated a less complete set of activities, but we normally tried to make use of all instruments for each target.

[9] Similar observations were made for soil targets, although the RAT was not normally used on soil. A particularly effective form of soil campaign was executed by turning the rover's front steering wheels inward and yawing the vehicle while counter-rotating one wheel to excavate a trench [*Arvidson et al.*, 2004]. Trenching allowed investigation of soil with remote sensing and IDD instruments down to depths of $\sim$10 cm.

3. Mission Narrative

[10] This paper covers Opportunity's exploration of the surface of Mars from landing on Sol 1 through the nominal mission (Sol 90), the first extended mission (Sols 91–180) and into the second extended mission up to Sol 511. Figure 1 shows a high-level timeline of rover activities during the mission, and Figures 2a–2c show maps of the rover's traverse from landing until Sol 511. Table 2 provides a more detailed sol-by-sol summary of rover activities. Table 3 summarizes the major rock campaigns, and Table 4 summarizes the major soil campaigns.

[11] Opportunity came to rest in Eagle crater, and the first images obtained by the rover revealed that an outcrop of layered bedrock was exposed in the crater wall less than 10 meters from the lander (Figure 3). The area immediately around the lander was clear of obstacles, allowing egress onto the Martian surface on Sol 7. The focus of subsequent activities within Eagle crater was on detailed remote sens-

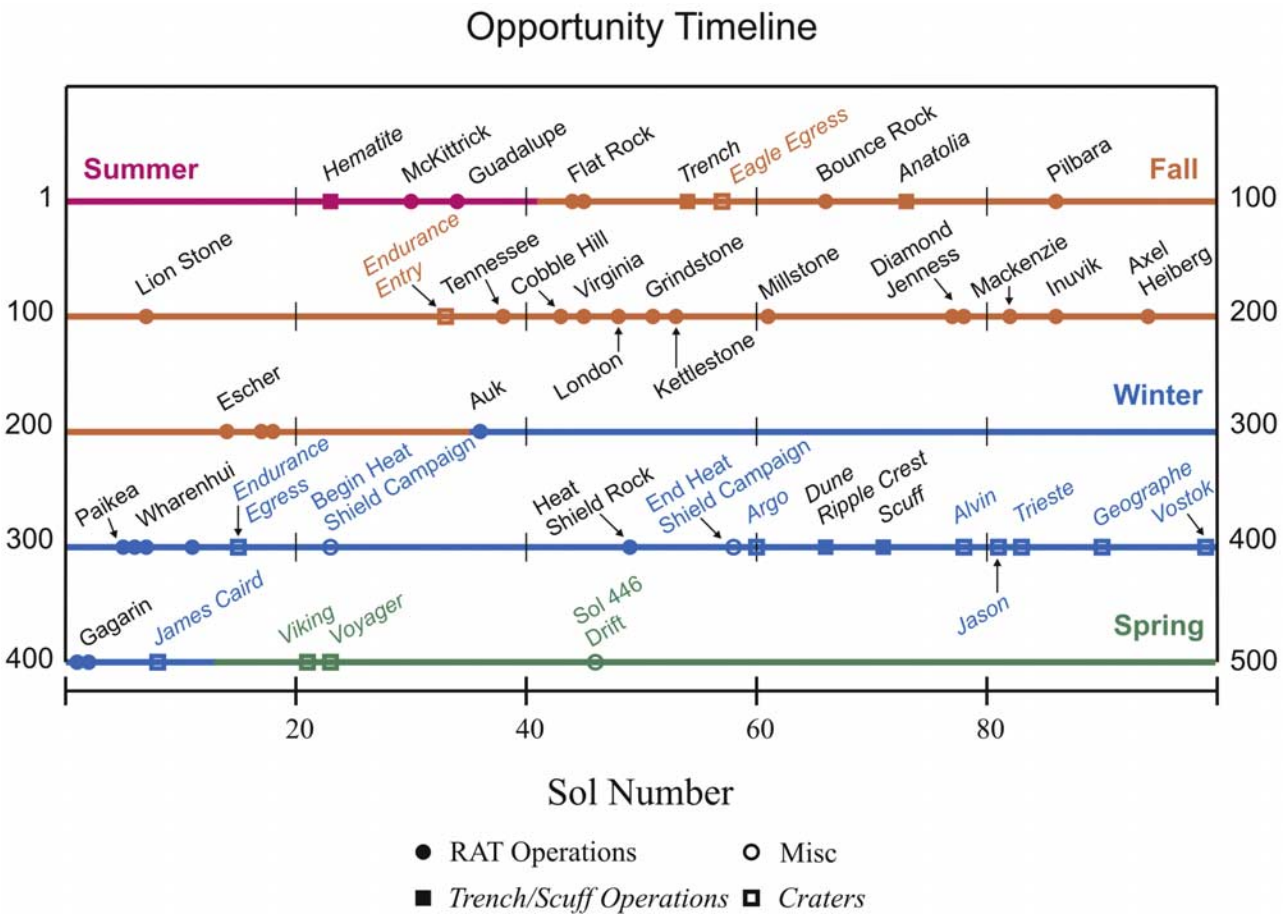

Figure 1. Opportunity mission timeline.

ing and in situ investigation of the outcrop materials. As a secondary objective, we also studied soil exposures within the crater, including excavation of a trench. On Sol 57 Opportunity exited Eagle crater and headed east on the Meridiani plains.

[12] The goal of the eastward drive was Endurance crater, a substantially larger impact crater about 800 meters away that we suspected would expose more stratigraphic section than was accessible at Eagle crater. Shortly after leaving Eagle crater we stopped to investigate Bounce Rock, a conspicuous rock on the plains near an airbag bounce mark. Brief additional stops were made on the way to Endurance crater to investigate a shallow trough, Anatolia, that appeared to be the surface expression of a fracture in the underlying bedrock, to conduct another trenching experiment, to visit the small, fresh impact crater Fram (Figure 4), and to conduct a photometry campaign on the plains between Fram and Endurance.

[13] On Sol 95 Opportunity arrived at Endurance crater (Figure 5). Endurance crater is approximately 150 m in diameter and 20 m deep, and it exposes in its walls a substantially thicker stratigraphic section than is available at Eagle crater. We began the investigation of Endurance crater by obtaining large Pancam and Mini-TES panoramas from a point on the western rim. Opportunity then traversed roughly 120 degrees counter-clockwise around the crater to a new position on the southeast rim and obtained another panorama there. Primary objectives for these panoramas were to map the interior of the crater for traverse planning purposes, and to try to find a place where Opportunity could safely enter the crater.

[14] Simultaneously with the traverse and imaging along the crater rim, the MER engineering team performed Earth-based rover testing that demonstrated Opportunity's ability to descend and climb slopes of up to about 30° on rocky surfaces. These test results, and the identification of an entry path consistent with the newly demonstrated rover capabilities, led to the decision to enter the crater. The entry point chosen was Karatepe West, along the crater's southwestern rim. Along with providing slopes that Opportunity was capable of descending, Karatepe West also offered thick exposures of layered bedrock (Figure 6). As an additional benefit, the north-facing slopes there tilted Opportunity's solar arrays toward the sun during the southern hemisphere winter, substantially increasing the arrays' power output.

[15] Opportunity entered Endurance crater on Sol 134, and over a period of several Earth months, descended down the southwestern wall of Endurance crater. Remote sensing observations were used to characterize the stratigraphy as the rover progressed, and we stopped for detailed in situ observational campaigns at each new stratigraphic unit. A total of eleven RAT holes were emplaced over a stratigraphic section of more than 7 meters, comprising the first strati-

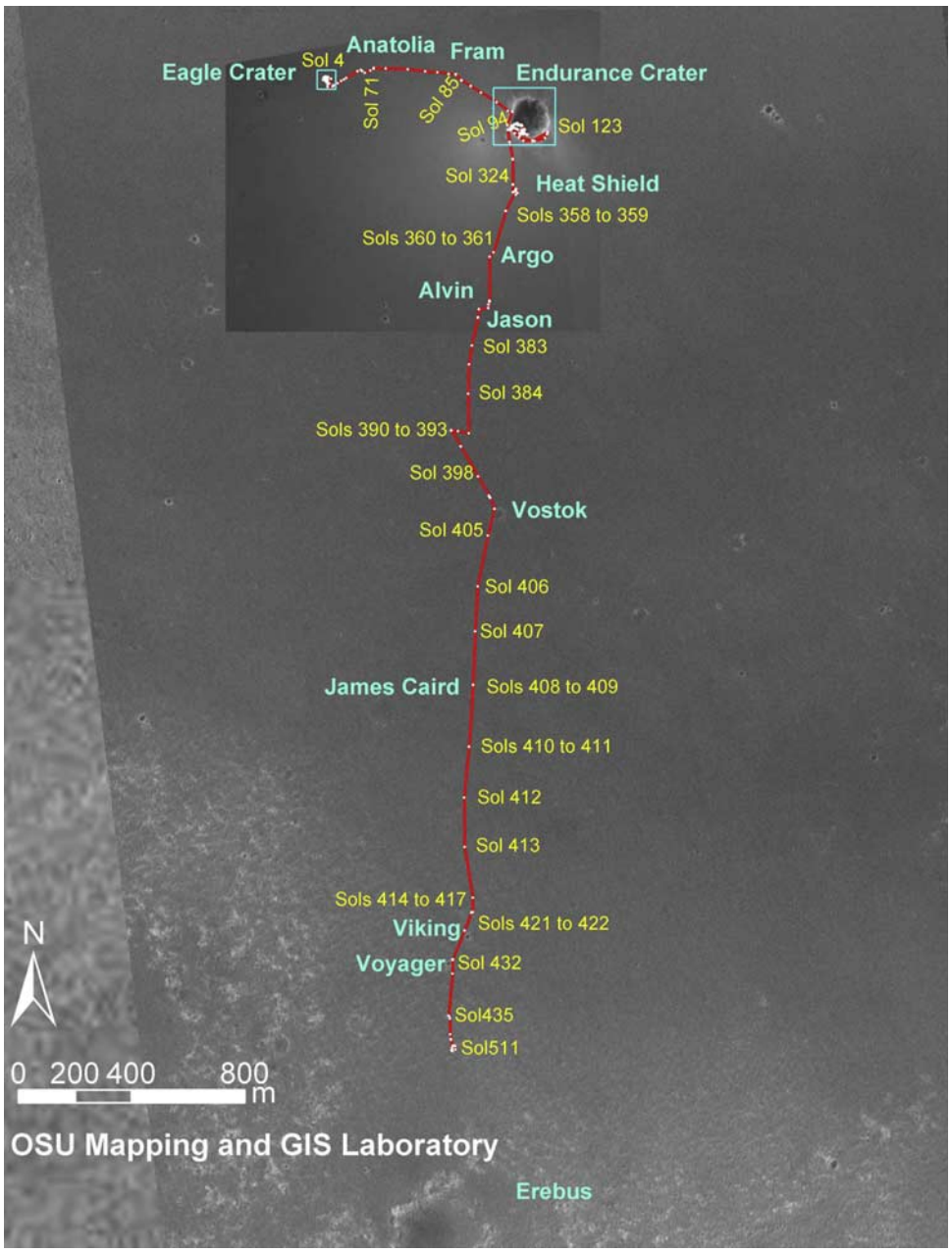

Figure 2a. Opportunity's traverse from landing to Sol 511. Base image was acquired by MGS MOC; inset near Eagle and Endurance craters was obtained during descent by the MER lander.

graphic section investigated in situ on another planet. Comprehensive measurements were made at each RAT hole with all IDD instruments (Table 3).

[16] The floor of Endurance crater is dominated by a striking dune field (Figure 7). Soft soil near the dunes that threatened to trap the rover prevented us from making in situ measurements of dune materials, so we focused instead on remote sensing observations. After leaving the crater floor we began to ascend toward a steep section of the southern crater wall that we named Burns Cliff, pausing for several rock and soil investigations along the way. The ascent to the base of Burns Cliff provided the ability to image the rocks there at close range (Figure 8) and to conduct additional in situ observations. Opportunity then traversed back to the Karatepe region, exiting Endurance crater at Karatepe East on Sol 315.

[17] With the investigation of Endurance crater complete, we directed Opportunity southward. Our eventual goals in this direction included mottled terrain that we suspected might expose more bedrock, and Victoria crater, an impact crater nearly 1 km in diameter. These goals, however, lay at distances of several km or more, requiring a substantial southward traverse.

[18] The first major stop along this traverse was at Opportunity's heat shield, which had been dropped from the lander during the descent to the surface. The primary

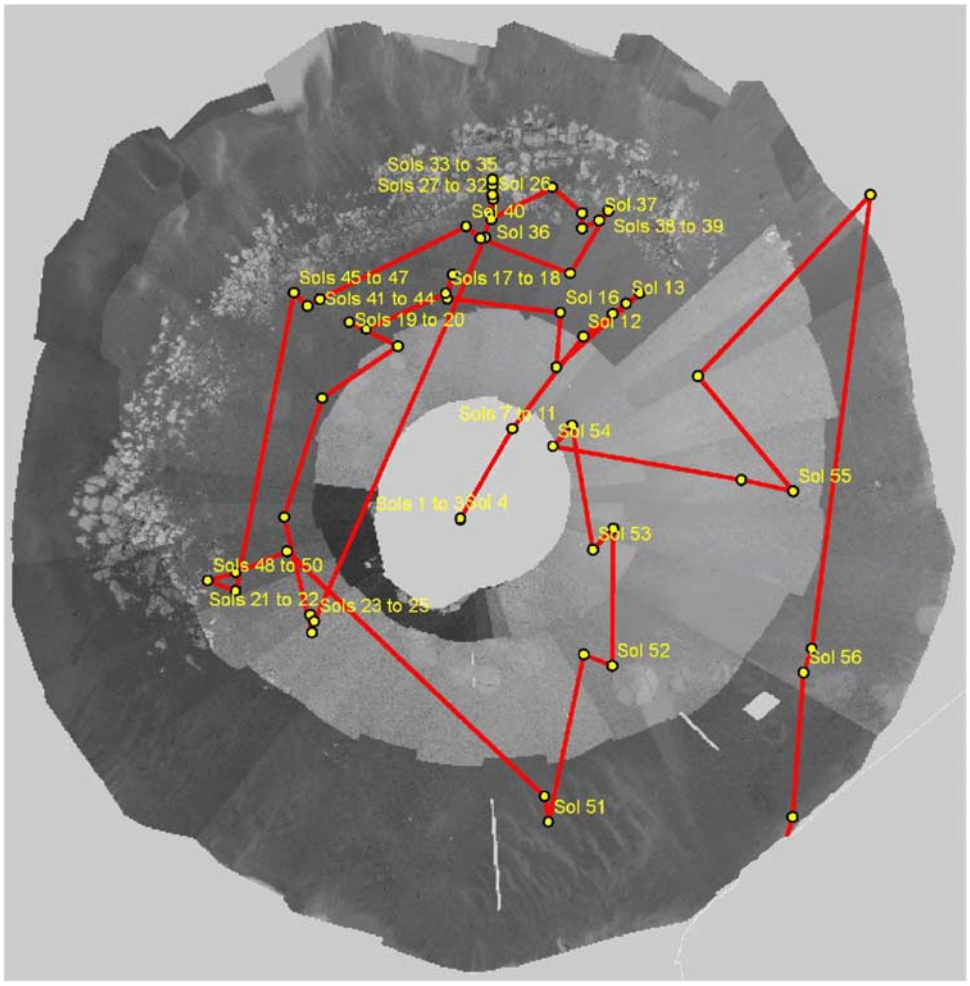

Figure 2b. Opportunity's traverse within Eagle crater. Base image is a Navcam mosaic obtained while the rover was still on the lander.

goal of the heat shield investigation was to assess the heat shield's engineering performance during the hypersonic atmospheric entry phase of the mission. While there we also discovered and performed detailed observations of Heat Shield Rock (Figure 9), an unusual loose rock on the plains that proved to be an iron meteorite.

[19] Opportunity left the heat shield on Sol 358 and began a very long southward drive. Our strategy for this drive was dubbed "crater hopping": traversing from one small impact crater to the next. These craters offered widely spaced probes of bedrock along the route, and also provided unambiguous landmarks that made it easy to localize the rover on plains that were otherwise nearly devoid of unique topographic features. Because the craters varied in age and hence degree of preservation, they also provided the opportunity to study the variety of crater morphology present and the degradation processes involved [*Grant et al.*, 2006]. An upload of new flight software to the rover briefly interrupted the drive on Sol 374. The largest crater along the route was Vostok, a feature about 40 meters in diameter that has undergone substantial erosion and infilling (Figure 10). Opportunity arrived at Vostok on Sol 399. After in situ measurements there, Opportunity continued southward toward and beyond the next major landmarks, a pair of craters named Viking and Voyager.

[20] Throughout the traverse we observed eolian ripples on the Meridiani plains, and these ripples increased in size as the rover got farther south. Our strategy for driving the very long distances that this traverse required involved turning off many of the safeguards that the rover can use to assess problems like wheel slip and sinkage. This strategy served us well for several kilometers, including traverses across many large ripples. However, on Sol 446, after leaving the vicinity of Viking and Voyager craters, a planned drive ended with all six rover wheels deeply embedded in a ripple ~30 cm high. Unlike previous encounters with similar features, Opportunity's wheels had sunk into this feature rather than cresting over it, and postdrive analysis showed that the rover had executed ~50 meters worth of wheel turns while making no forward progress. We later came to name this feature Purgatory Ripple (Figure 11).

[21] Extraction of Opportunity from Purgatory Ripple took several weeks. Much of this time was spent performing Earth-based testing in analogs of Martian soil, attempting to find the optimal technique for extracting the

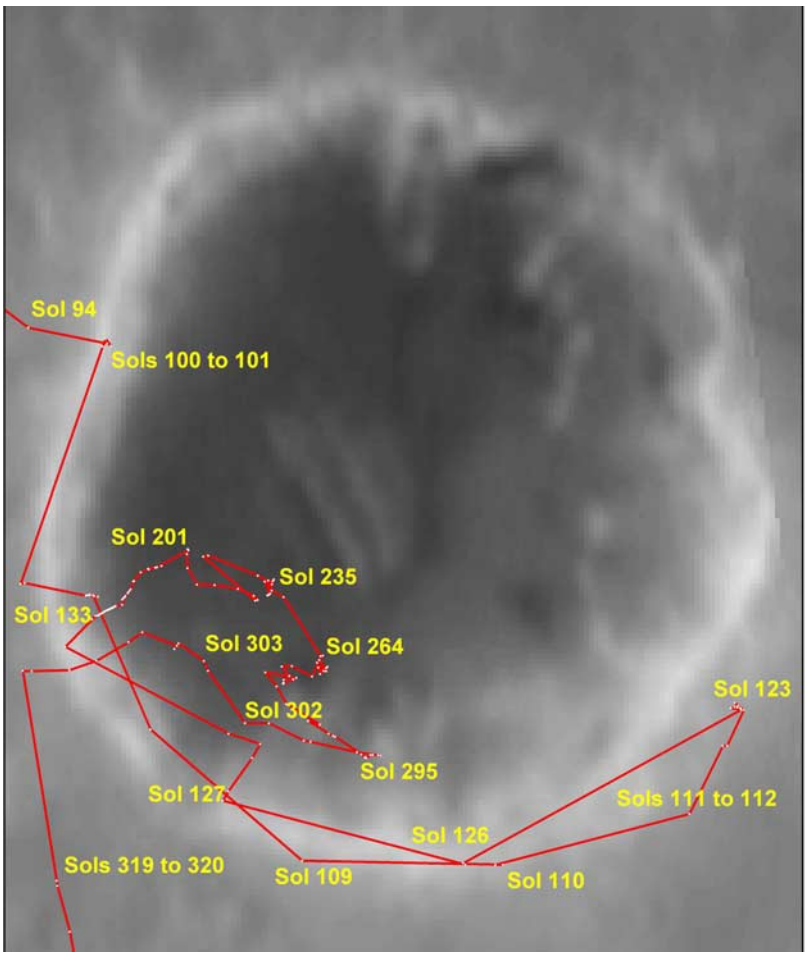

Figure 2c. Opportunity's traverse within Endurance crater. Base image was acquired by MGS MOC.

rover from deep sand. While this work was underway, we used Pancam to obtain a very high resolution multispectral panorama that we named the Rub-al-Khali Pan, as well as an extensive photometry experiment. Extraction of the rover from Purgatory Ripple began on Sol 461, and after 192 meters of commanded wheel turns Opportunity was finally freed from Purgatory on Sol 484. We spent the remainder of the time covered by this paper, up to Sol 511,

Table 2. Summary of Rover Activities From Landing to Sol 511[a]

Sols	Description of Activities	Site at Start of Sol
001–002	EDL, lander-based RS	0
003–006	lander-based RS	2
007	egress	2
008–011	tarmac soil target, IDD, targeted RS	2
012	drive to outcrop target Snout	2
013–014	snout IDD and RS	3
015	Robert E IDD and RS	3
016–17	drive to Alpha and Bravo features	3
018	anomalies precluded science observations	3
019–020	Dark Nuts soil IDD, RS	3
021–022	drive to trench site, pretrench RS	3
022–023	MGS coordinated observations, IDD, trench, RS	4
024–025	IDD trench floor and walls	4
026–027	drive to El Capitan, targeted RS	4
028–029	Guadalupe pre-RAT in situ observations	4
030–032	McKittrick RAT, IDD	4
033–035	bump to Guadalupe, RS, IDD	5
036	backup, RS	5
037–039	drive to Last Chance, RS, soil in situ measurements, Mars Express coordinated observations	5
040	IDD, RS, drive to Wave Ripple	5
041–043	drive to Berry Bowl, IDD, RAT attempt on Flat Rock	5
044–045	Flat Rock RAT, IDD, RS, RAT brush, IDD, RS	5

Table 2. (continued)

Sols	Description of Activities	Site at Start of Sol
046–047	Berry Bowl IDD, RS, Magnet observations	5
048	drive toward Shoemaker's Patio, RS	6
049–050	bump to Shark's Tooth, IDD, RS	6
051–053	scuff on Carousel, RS, drive to soil target, touch and go, magnet observations	6
054	trench excavation, RS of trench, drive to crater rim	6
056	attempt to egress Eagle Crater	7
057–058	egress Eagle Crater, RS	8
059–062	drive toward Bright Spot, IDD, RS, Pancam Lion King Panorama, drive along crater rim, RS	8
063	drive to Bounce Rock	8
064	science stand-down	8
065–069	Bounce Rock IDD, RS, RAT, soil in situ measurements	8
070–071	"crush and go" on Bounce Rock and drive to Anatolia	9
072–073	Anatolia final approach, trench, RS	10
075–079	science stand-down for software upload	10
079–080	Anatolia trench observations, IDD, RS, APXS calibration	10
081–084	drive toward Fram Crater (600-meter mission success distance achieved), RS, IDD	11–14
085–087	drive to Pilbara, RAT, IDD, RS	14
088–090	drive to plains, photometry experiment	15
091	targeted RS	16
092–095	drive to Endurance Crater	17–20
096–102	Endurance Crater Rim RS	20–21
103–108	drive to Lion Stone, IDD, RAT, post-RAT IDD, RS of heat shield	22–23
108–111	drive along southern edge of Endurance	25–26
112	DSN error resulting in low battery state of charge, RS of crater rim.	27
113	battery charge	28
114–122	drive to crater edge, RS, Pancam panorama	28
123–126	McDonnell, Pyrrho, Diogenes IDD	28–29
127–132	mobility test, drive toward Karatepe, RS to assess possible ingress point	30–31
133	executed "dip" into Endurance Crater	31
134–137	drive into crater, approach Tennessee, RS	31
138–141	Tennessee IDD, RAT, RS	31
142–144	Bluegrass, Siula Grande, Churchill, Cobble Hill IDD, RAT	31
145–150	Virginia, London IDD, RAT	31
151–154	Grindstone, Kettlestone IDD, RAT, RS	32
155	arm calibration activity on Grindstone, Kettlestone, and backup	32
156	failed upload due to time conversion error, minimal science activity	32
157–158	RS, drive to 6th layer, maneuver to get all wheels on ground	32
159–163	RS, Millstone, Drammensfjorden IDD, RAT, diagnostic tests on APXS doors	32
164–166	My_Dahlia IDD, RS	32
167–168	capture magnet data, RS	32
169–172	drive to Razorback	32–33
173–174	Arnold Ziffel IDD, RS	33
175–176	RS, drive to Diamond Jenness	33
177–180	Diamond Jenness IDD, RAT (2 depths), backup, RS	33
181–183	Razorback IDD, drive to Mackenzie, RAT, IDD, backup, RS	33
184–185	Mackenzie RS, drive to Inuvik, bump to get Tuktoyuktuk target in IDD work volume	34
186–187	Tuktoyuktuk IDD, RAT	34
188–192	drive to Axel Heiberg, MI diagnostics, RS	34
193–197	Axel Heiberg IDD, RAT, RS	35
197–198	Sermilik IDD	35
199	Jiffypop	35
200	anomaly precludes science observations	35
201–202	drive toward dune tendril, RS	35
203–204	drive to Shag target on Ellesmere	35
205	drive to Auk target on Ellesmere	35
206–210	drive to Escher, IDD, diagnostic image of RAT	35
211	Kirchner IDD, thermal inertia measurements on dunes	35
212	RAT calibration, Mini-TES-IDD simultaneous operation experiment	35
214–218	EmilNolde, Kirchner_RAT, and Otto Dix IDD, RS, RAT brush	35
219	load solar conjunction sequences	35
220–222	Kirchner IDD, Escher RS, Spherules near Auk IDD, RS	35
223–235	Conjunction sequence, Spherules near Auk IDD	35
236–241	drive to Auk. Auk, Ellesmere, Barbeau IDD, RS (transition to 5 day/week planning)	35
242–243	drive to Miro	36
244–245	Lyneal, Llangollen, and Platt Lane targets on Welshampton feature IDD, RS	36
246–248	void target on Rocknest feature IDD, RS	36
249–257	drive to Wopmay, approach and RS	36
258–263	Wopmay targets IDD, RS	36
264–272	drive toward Burns Cliff, slip errors and mobility testing, RS	37
273–274	filter magnet observations, drive toward Burns Cliff, RS	37
275–279	drive toward Burns Cliff, capture magnet observations, RS	37
280–285	Wanganui IDD, RS, continue drive toward Burns Cliff	37
286–294	Burns Cliff RS	37

Table 2. (continued)

Sols	Description of Activities	Site at Start of Sol
295–297	drive west, investigate possible egress chute, IDD, RS	38
298–304	drive toward Karatepe	38
305–306	Paikea IDD, RAT, Wharenhui, Paikea, and Contact RS	38
307–311	Wharenhui IDD, MGS overflight experiment	38
312–314	drive to crater rim egress location, RS	38
315	egress from Endurance Crater	39
316–319	drive to tracks, IDD, RS	39
320–324	drive toward heat shield, RS	39–40
325–326	RS of heat shield debris field from West Point and South Point	40
327–330	compositional cal target, capture magnet IDD, RS	40
331–337	drive to Flank Target, IDD, RS, capture magnet in situ observations	40
338–340	drive toward fractured edge of heat shield	40
341–344	IDD on fractured edge of heat shield, magnet observations, RS, in situ observations of filter magnet	40
345–346	drive to Heat Shield Rock, RS	40
347–352	Heat Shield Rock IDD, RAT brush, RS	40
353–355	drive to heat shield	40
356	heat shield; IDD	40
357	thermal inertia measurements	40
358–364	drive toward Argo	40–41
365	Strange Rock RS	42
366–370	trench on dune ripple crest, IDD, RS	42
371–373	scuff, bump back, IDD, RS	42
374–376	software upload	42
377–378	drive, RS, test new software	43
379–382	Russet IDD, Jason RS	43
383–386	drive toward crater, RS	43
387–391	drive to crater triplet; RS	44–47
392–394	Normandy IDD, RS	47
395–399	drive toward Vostok	47–49
400–405	Laika, Gagarin IDD, RAT, RS	50
406–414	drive south, RS	50–51
415–417	Mobarak IDD, RS in trough	52
418–420	Norooz, Mayberooz IDD top of ripple	52
421–422	drive to Viking, RS	52
423–424	drive to Voyager, RS	52
425	Mars Odyssey in safe mode, DTE established	52
426–427	RS and atmospheric observations, DTE pass only	52
428–439	drive south, RS, diagnostics on right front steering actuator	52–54
440	software reset during Mini-TES observation	55
441–442	recovery and diagnostic testing	55
443–445	soil campaign, IDD, RS	55
446	drive ended with all 6 wheels imbedded in 30 cm ripple	55
447–455	testbed activities to develop extraction plan	55
456–460	Rub al Khali panorama	55
461–484	extraction of the rover from Purgatory Ripple	55
485–489	RS of Purgatory Ripple	55
490	drive away from Purgatory Ripple	55
491–493	DSN error, uplink for 3-sol plan did not occur	55
494–497	turn toward Purgatory Ripple, RS	55
498	North Dune IDD	55
499–504	drive into position on Purgatory Ripple, RS	55
505–510	Purgatory Ripple IDD, RS	55
511	drive south	55

[a]EDL, entry, descent and landing; RS, remote sensing; IDD, Instrument Deployment Device (i.e., use of Microscopic Imager, Mössbauer Spectrometer, and/or APXS); RAT, Rock Abrasion Tool; DTE, direct to Earth.

investigating Purgatory Ripple and the deep tracks made there by the rover.

4. Results

4.1. Bedrock

4.1.1. Sedimentology and Stratigraphy

[22] Early observations by Opportunity at Eagle crater enabled some noteworthy sedimentological findings [*Squyres et al.*, 2004b], but the observations were difficult to put into context because of the small amount of stratigraphic section exposed. This paucity of section motivated the traverse to Endurance crater, which was amply rewarded with the observations made at Karatepe West. We have named the stratigraphic unit exposed at Karatepe west and elsewhere the Burns formation.

[23] Primarily on the basis of the observations at Karatepe West, we divide the Burns formation into distinct lower, middle, and upper units [*Grotzinger et al.*, 2005]. All three units are observed or inferred to be sandstones, formed from sand grains that are rich in a variety of sulfate salts.

[24] The lower unit of the Burns formation was not sampled directly at Karatepe West, but was observed using Pancam and Mini-TES at the eastern end of Burns Cliff.

Table 3. Summary of Major Rock Campaigns

Feature/Target Names and RAT Operations	Brief Description
Eagle Crater	
McKittrick/Middle_RAT (4.3 mm grind) (Sols 30–32)	outcrop
Guadalupe/King3 (4.9 mm) (Sols 28–29)	outcrop
Flat Rock/Mojo2 (3.1 mm) (Sols 41–43)	outcrop
Bounce Rock/Case (6.4 mm) (Sols 65–69)	float, probable distant impact ejecta
Fram Crater	
Pilbara/Golf (7.2 mm) (Sols 85–87)	outcrop
Endurance Crater	
Lion Stone/Puma (6.3 mm) (Sols 103–108)	float, probable Endurance crater ejecta
Tennessee/Vols (8.1 mm) (Sols 138–141)	outcrop
Kentucky/Cobble Hill (3.8 mm) (Sols 142–144)	outcrop
Layer-C/Virginia (4.3 mm) (Sols 145–149)	outcrop
Layer-D/London (4.5 mm) (Sols 145–149)	outcrop
Manitoba/Grindstone (2.7 mm) (Sols 151–154)	outcrop
Manitoba/Kettlestone (4.2 mm) (Sols 151–154)	outcrop
Millstone/Drammensfjorden (6.3 mm) (Sols 159–163)	outcrop
Diamond Jenness/Holman_3 (~2 mm on sol 177, then 5.0 mm on sol 178) (Sols 177–180)	outcrop
Mackenzie/Campbell_2 (8.4 mm) (Sols 181–183)	outcrop
Inuvik/Tuktoyuktuk_2 (7.7 mm) (Sols 184–185)	outcrop
Bylot/Aktineq (7.7 mm on Sol 194)	outcrop
Escher/Kirchner (7.3 mm on Sol 218) (Sols 206–210)	float
Auk/Auk_RAT (brush sequence in soil, faulted on pebble) (Sol 236)	soil (this was the one instance of use of the RAT on soil)
Black Cow/Paikea (6.3 mm) (Sols 305–306)	outcrop
Black Cow/Wharenhui (2.1 mm) (Sols 305–306)	outcrop
Heat Shield Rock/Squidward (brushed on Sol 349)	meteorite
Yuri/Gagarin (6.0 mm) (Sols 400–405)	outcrop

There it forms a spectacular cross bed set, more than 1.5 m thick, that is truncated and disconformably overlain by the middle unit. Low-angle truncations are abundant within the lower unit. On the basis of these observations, we concluded that the lower unit was formed by migrating sand dunes [*Grotzinger et al.*, 2005]. The unit could not be observed with the Microscopic Imager due to concerns about rover safety on the steep slopes encountered; therefore grain sizes remain unknown for this bed.

[25] The contact between the lower and middle units, which is well exposed at the eastern end of Burns Cliff, is interpreted as an eolian deflation surface. Above this contact, the middle unit consists of sandstones that exhibit distinctive fine planar lamination in some locations and low-angle cross-lamination in others. (As noted below, however, lower portions of the middle unit have been so severely recrystallized that lamination is commonly obscured.) Grain sizes typically range from 0.3–0.8 mm within the middle unit; many laminations are only a single grain thick and are composed of grains that are well sorted within laminae. On the basis of these characteristics, the middle unit is interpreted to be a sand sheet deposit that accumulated as eolian impact ripples migrated across a nearly flat-lying sand surface.

[26] The contact between the middle and upper units is diagenetic rather than sedimentological in origin. Substantial recrystallization is evident in Microscopic Imager images immediately below the contact [*Grotzinger et al.*, 2005, *McLennan et al.*, 2005], while much less recrystallization is seen above it. There are also distinct transitions in elemental chemistry (and inferred transitions in mineralogy) that are consistent with enhanced diagenetic modification below the contact [*McLennan et al.*, 2005, *Clark et al.*, 2005].

[27] Like the middle unit, the lower reaches of the upper unit are also dominated by fine-scale planar lamination and low-angle cross-lamination indicative of origin as a sand sheet. In the upper portion of the upper unit, however, there is a distinct change in sedimentological character. The sandstones there are distinguished by wavy bedding and, most notably, by small-scale festoon or trough cross lamination. This cross lamination, first described at Eagle crater [*Squyres et al.*, 2004b] and subsequently also observed in what we believe to be correlative beds at Karatepe West [*Grotzinger et al.*, 2005], is interpreted at both locations to result from ripple migration induced by surface flow of liquid water over sand.

[28] Taken together, these observations point to an origin of the explored portion of the Burns formation as a "wetting upward" succession from dry eolian dunes to wet interdune deposits. The lower unit represents the dunes themselves, and the upper portion of the upper unit represents sediments transported in water that pooled on the surface, perhaps between dunes. The sand sheet of the middle unit and the lower portion of the upper unit is transitional, perhaps

Table 4. Summary of Major Soil Campaigns

Name	Brief Description
Hematite	trench on Sol 23, Hematite rich soil in Eagle Crater for stratigraphy, roughly 8 cm
Trench Site	trench on Sol 54, Eagle Crater, White material in ripple area
Anatolia	trench on Sol 73, near Anatolia trough outcrop area with ripple material
Dune Ripple Crest	scuff then Trench on Sol 366, Ripple crest material, outside Endurance Crater past heat shield
Ripple Campaign	eolian ripple crest and valley MI, MB, APXS Mobarak, Nobrooz, Mayberooz, Sols 415–420
Purgatory Ripple	characterization of Purgatory Ripple material, Sols 446–515

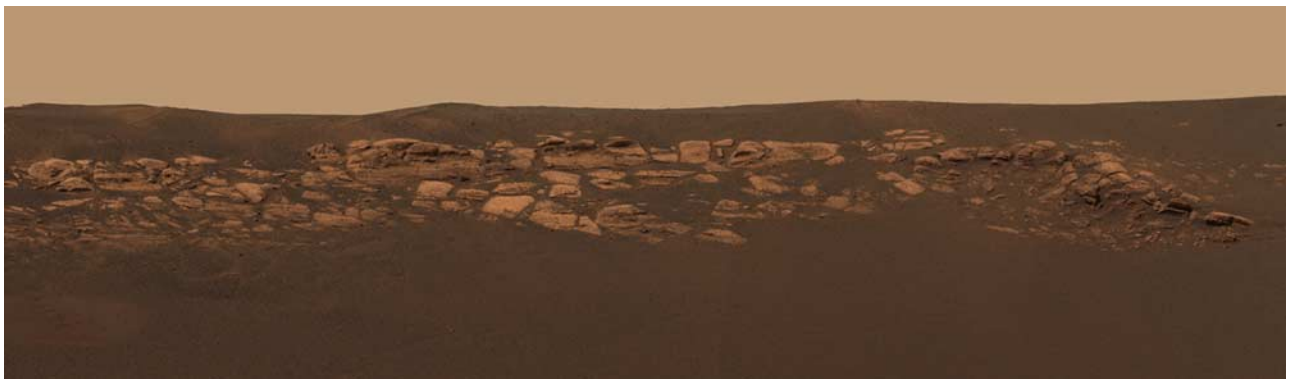

Figure 3. Approximate true color Pancam panorama of outcrop rocks exposed in the wall of Eagle crater. Image acquired while Opportunity was still on the lander.

representing the margin between dry dune and wet interdune deposits.

4.1.2. Geochemistry and Mineralogy

[29] Mössbauer, APXS, Mini-TES and Pancam spectra collectively indicate that the outcrop matrix throughout all explored portions of the Burns formation contains three main components: silicate minerals, sulfate salts, and oxidized iron-bearing phases, especially hematite [*Squyres et al.*, 2004b; *Clark et al.*, 2005]. Cation abundances show that outcrop chemistry derives from chemical weathering of a precursor olivine basalt [*Squyres et al.*, 2004b; *Clark et al.*, 2005; *Tosca et al.*, 2005], but electrochemical balance with constituent anions requires that a high proportion of these cations now resides in sulfate (and perhaps minor chloride) minerals. Consistent with this observation, Mössbauer spectra of outcrop surfaces brushed and abraded by the RAT show no evidence of either olivine or magnetite, although these and other Fe-bearing basaltic minerals show up clearly in the unconsolidated sands that are ubiquitous on the Meridiani plains [*Klingelhöfer et al.*, 2004; *Morris et al.*, 2006]. (Mini-TES does detect olivine in some observations targeted on outcrop material, but the source of this olivine signal is the basaltic sand that is commonly strewn on outcrop surfaces at scales smaller than Mini-TES' spatial resolution [*Christensen et al.*, 2004; *Glotch and Bandfield*, 2006]. Multispectral visible and near infrared observations of the Meridiani outcrop and basaltic sands also indicate that they are very distinct materials (Farrand et al., submitted manuscript, 2006). Al and Si co-vary across all of the outcrop samples analyzed to date, with Si in excess of Al, suggesting that both aluminosilicate minerals (clays?) and a nonaluminous silicate, possibly free silica, occur as fine-grained components of the outcrop matrix [*Clark et al.*, 2005]. Linear deconvolution of Mini-TES spectra of outcrop material [*Glotch and Bandfield*, 2006] indicates that it is composed of ~25% amorphous silica. Linear deconvolution also yields ~15% oligoclase, a Na-rich plagioclase feldspar, and ~10% nontronite, which is considered a tentative detection [*Glotch et al.*, 2006b].

[30] One key sulfate mineral group identified by Opportunity's instruments is jarosite [*Klingelhöfer et al.*, 2004; *Morris et al.*, 2006], predominantly H_3O^+-jarosite, to judge from cation abundances [*Clark et al.*, 2005]. Jarosite is environmentally informative, because it is known to precipitate only from acidic solutions. Sulfuric acid, possibly formed by reaction of sulfur-bearing volcanic gases with water vapor or the products of its photolytic dissociation, must have exerted a strong influence on basalt weathering and sediment deposition at Meridiani Planum [*Burns*, 1986, 1987]. That jarosite still persists in outcrop indicates that these rocks have not seen substantial amounts of water with pH above 4–5 since their formation [*Madden et al.*, 2004; *Tosca et al.*, 2005; *Fernandez-Remolar et al.*, 2005].

[31] Consistent with Mini-TES observations of the outcrop that reveal evidence for Mg- and Ca-sulfates [*Christensen et al.*, 2004; *Glotch et al.*, 2006b], cation abundances measured by APXS [*Rieder et al.*, 2004] require that Mg-sulfates dominate the sulfate component, with subordinate amounts of Ca-sulfate minerals and jarosite [*Clark et al.*, 2005]. Additional sulfate minerals may be present in the

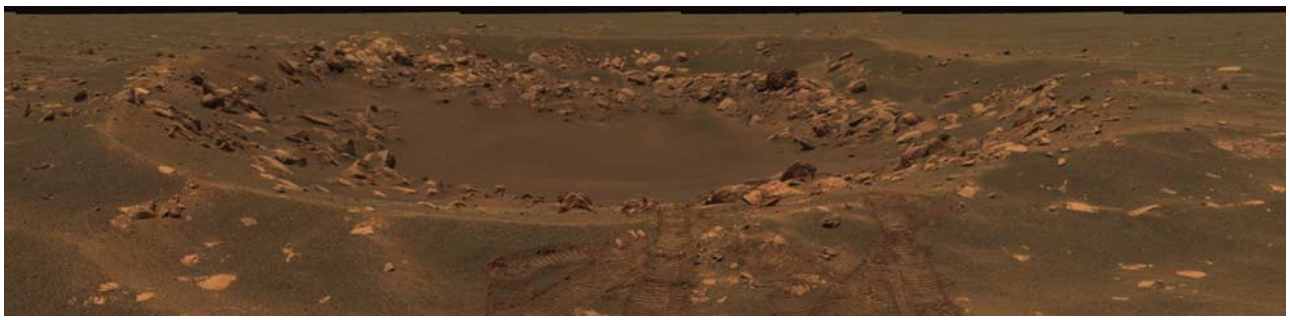

Figure 4. Approximate true color Pancam panorama of Fram crater. Image acquired on Sol 88.

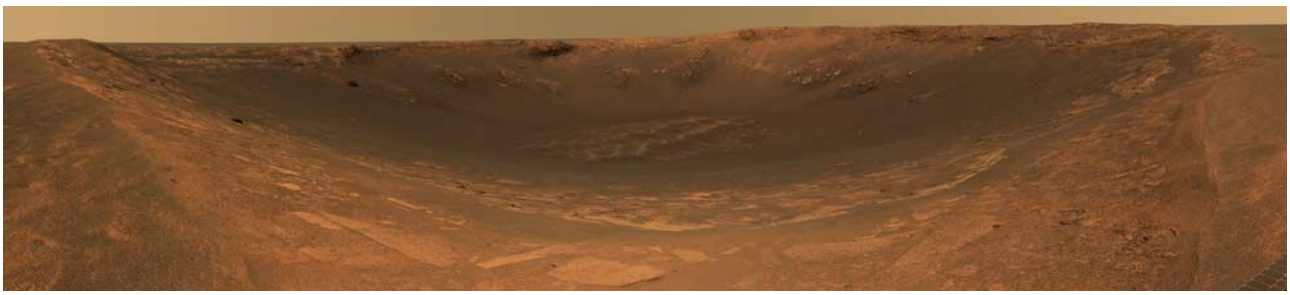

Figure 5. Approximate true color Pancam panorama of Endurance crater. Image acquired on Sols 97 and 98, from Opportunity's first point of arrival on the western rim of the crater.

ferric component identified in Mössbauer data only as Fe_3D_3 (see below), one candidate being schwertmannite (Farrand et al., submitted manuscript, 2006). Linear deconvolution of the Mini-TES outcrop spectral end-member, aided by mass balance constraints from APXS elemental abundances, yields ~20% kieserite, ~10% anhydrite, and 10% jarosite [*Glotch et al.*, 2006b]. Insofar as many of the identified or inferred sulfate minerals are hydrated, water of hydration in outcrop rocks is likely to be significant [*Squyres et al.*, 2004b], perhaps running between 1 and 5% by weight [*Clark et al.*, 2005; *Glotch et al.*, 2006a, 2006b]. Cl and Br abundances are low, but highly variable among samples, with Cl peaking in stratigraphically lower horizons at Karatepe West, while Br shows a statistically complementary distribution [*Clark et al.*, 2005]. The large variations in Cl/Br ratio within the outcrop at both Eagle and Endurance craters may be an indicator of fractionation of chloride and bromide salts via evaporative processes [*Squyres et al.*, 2004b, *Rieder et al.*, 2004]. Hematite makes up about 7% of the rock matrix [*Klingelhöfer et al.*, 2004; *Morris et al.*, 2006], and the hematite in the matrix helps lend a brick-red shade to the fine-grained cuttings produced when the RAT is used on outcrop surfaces [*Bell et al.*, 2004]. (A portion of the hematite in outcrops occurs in concretions, discussed below, but by weight, most must reside in the matrix.) A second ferric component present as ~4% by weight is the one identified in Mössbauer spectra as Fe_3D_3, a designation that refers to a suite of iron oxide and sulfate minerals that have overlapping and hence undiagnostic Mössbauer signatures [*Klingelhöfer et al.*, 2004]. Modern terrestrial environments where jarosite and iron oxides precipitate from acidic waters commonly include the ferric iron sulfate mineral schwertmannite among the Fe_3D_3 minerals [*Fernandez-Remolar et al.*, 2005]. Overwhelmingly, the iron present in outcrop minerals is ferric, indicating oxidizing conditions during deposition and diagenesis.

[32] Overall, geochemical data indicate that the matrix consists of silicate minerals derived by aqueous chemical alteration of olivine basalt mixed with sulfate minerals formed by the evaporation of ion-charged waters under acidic, oxidizing, and arid conditions [*Squyres et al.*, 2004b], and hematite precipitated by early diagenetic groundwaters in contact with primary depositional minerals [*McLennan et al.*, 2005; *Clark et al.*, 2005]. The mineralogy observed or inferred for Meridiani outcrop rocks compares closely with that expected during the evaporative evolution of waters formed during sulfuric acid weathering of olivine basalt [*Tosca et al.*, 2005].

4.1.3. Diagenesis

[33] The rocks at Meridiani underwent variable and in some cases substantial diagenetic modification after their

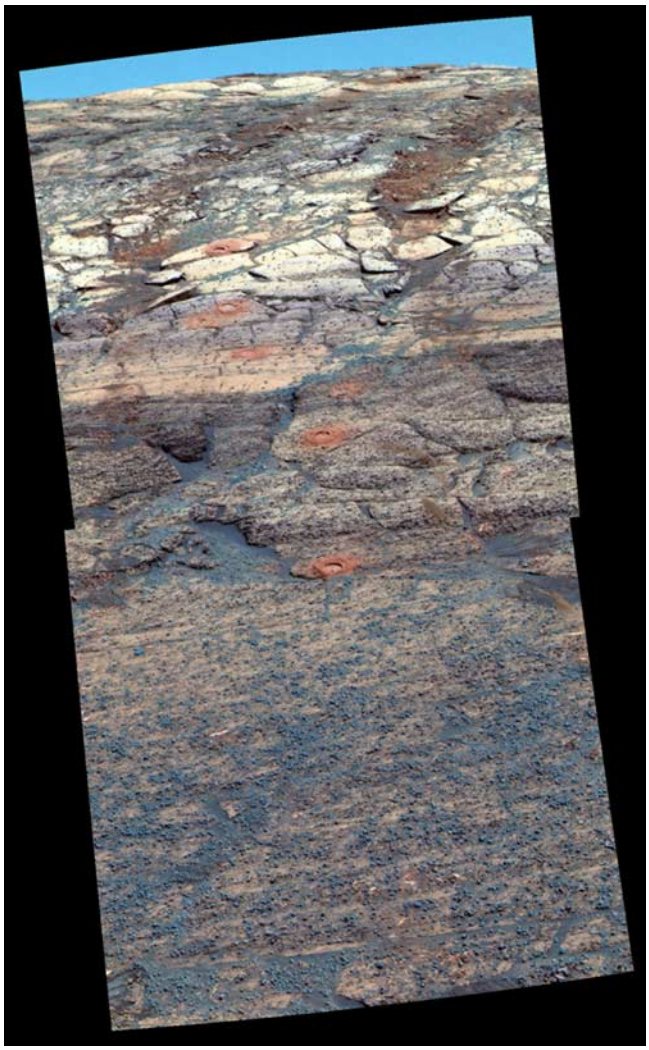

Figure 6. False color Pancam image of the upper portion of the stratigraphic section at Karatepe West, showing rover wheel tracks and seven of the eleven RAT holes made during the descent. Image acquired on Sol 173 using Pancam's 753 nm, 535 nm, and 432 nm filters, L2, L5, and L7.

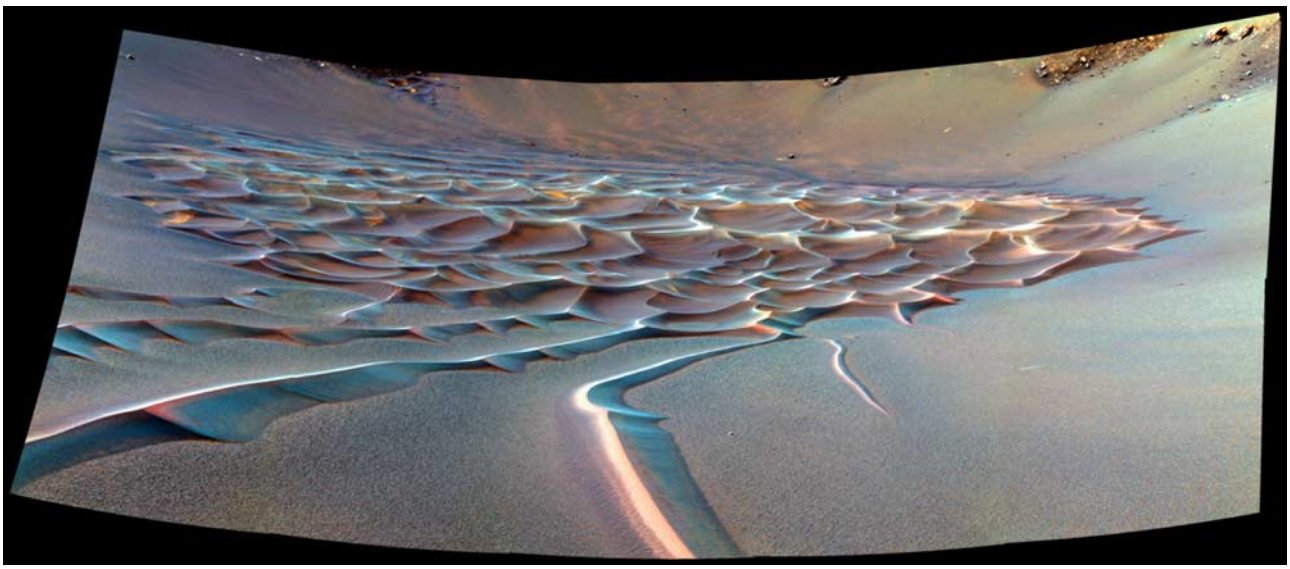

Figure 7. False color Pancam panorama of the dune field on the floor of Endurance crater. Image acquired on Sol 211 using Pancam's 753 nm, 535 nm, and 432 nm filters, L2, L5, and L7.

initial deposition [*McLennan et al.*, 2005]. Most conspicuous among diagenetic phases are the small spherules [*Squyres et al.*, 2004b], informally referred to as "blueberries," that are found in all outcrops observed at Meridiani to date. Blueberries play a major role in the development of an integrated understanding of Meridiani geology, not least because a surface veneer of these spherules, eroded from outcrop rocks, carries the remotely sensed spectral signature of hematite that motivated landing on the Meridiani plains [*Christensen et al.*, 2000, 2001; *Golombek et al.*, 2003; *Squyres et al.*, 2004a]. The volumetric distribution of blueberries in outcrop rocks is overdispersed (i.e., more uniform than random) and their shapes are almost perfectly spherical. These observations, along with the distinctive chemistry and mineralogy of the spherules, suggest that they are sedimentary concretions that formed diagenetically in stagnant or nondirectionally migrating groundwaters that saturated sulfate-rich Meridiani sands. Spherules are found abundantly in the eolian sandstones that dominate the lower and middle units of the Burns formation, and also in the water-lain sediments in the upper unit, indicating that groundwater percolated through all beds examined to date. The concretions developed in sandy sediments, but no granular texture is visible in their interiors at the resolution of the Microscopic Imager [*Herkenhoff et al.*, 2004]. This observation suggests both that solution was involved in their formation and that the insoluble siliciclastic fraction of outcrop rock is very fine-grained [*Squyres et al.*, 2004b].

[34] Mössbauer, APXS, Mini-TES and Pancam data all indicate that spherules consist primarily of hematite [*Klingelhöfer et al.*, 2004; *Rieder et al.*, 2004; *Christensen et al.*, 2004; *Bell et al.*, 2004; *Morris et al.*, 2006]. The high concentration of hematite in soils dominated by fractured

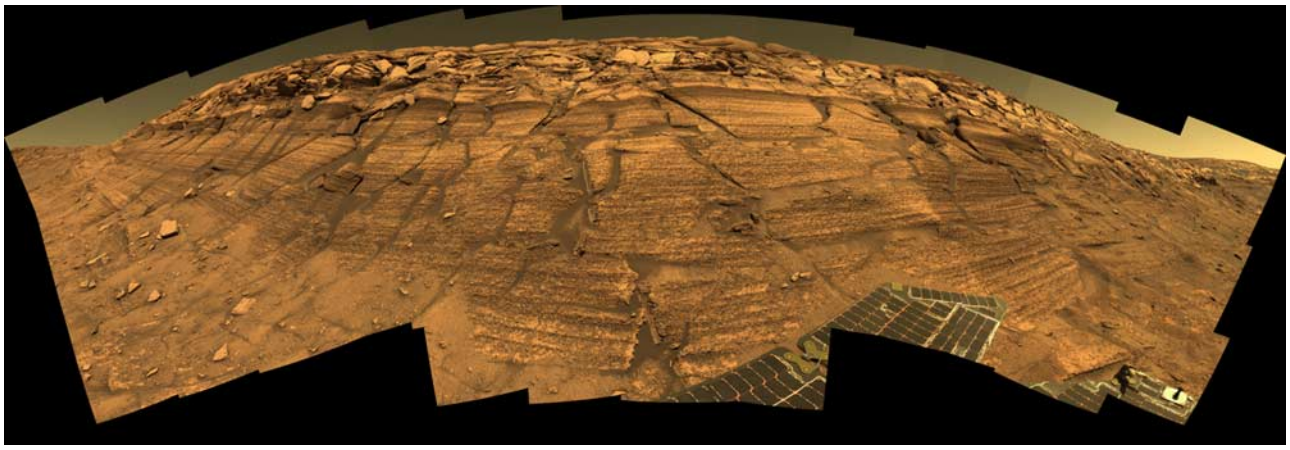

Figure 8. Approximate true color Pancam panorama of Burns Cliff. Image acquired on Sols 287 and 294, from Opportunity's position immediately at the base of Burns Cliff. Viewing direction is toward the southeast, so east is to the left. For high-resolution views of diagnostic sedimentary features here and elsewhere in the Burns formation, see *Squyres et al.* [2004b] and *Grotzinger et al.* [2005].

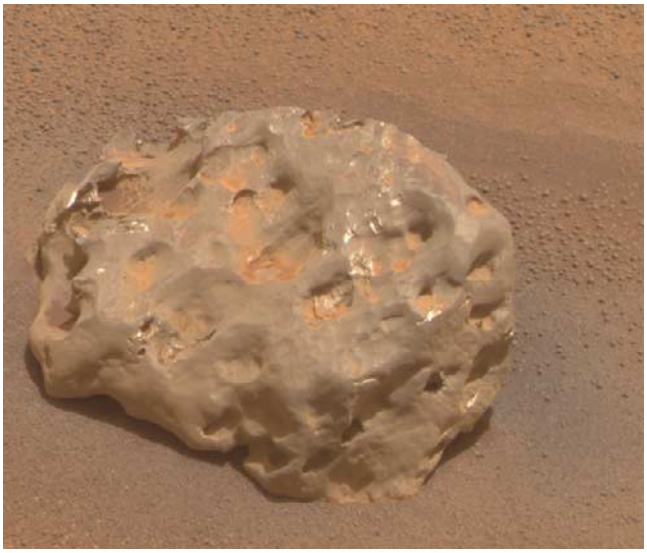

Figure 9. Approximate true color Pancam image of Heat Shield Rock. Image acquired on Sol 346.

spherules [*Klingelhöfer et al.*, 2004] and Pancam observations of spherules sectioned by the RAT [*Squyres et al.*, 2004a, 2004b] show that hematite concentration is high throughout the spherules, not just a surface coating. These observations are also consistent with the view that the concretions incorporated the fine-grained siliciclastic component of the outcrop matrix and dissolved more soluble sulfates as they grew [*McLennan et al.*, 2005]. Groundwater dissolution of jarosite may have provided the iron for hematite precipitation, but the fact that substantial amounts of jarosite remain in the rocks requires that diagenesis was strongly water-limited [*McLennan et al.*, 2005; *Madden et al.*, 2004; *Tosca et al.*, 2005; *Fernandez-Remolar et al.*, 2005]. Mini-TES spectra of Meridiani hematite most closely resemble those of laboratory samples derived by low-temperature conversion from goethite, rather than by formation of hematite at high temperature [*Glotch et al.*, 2004, 2006a]. While it is possible that hematite replaced a precursor goethite phase, it is not necessary to postulate this, as Fe^{3+} can be transported by and hematite can precipitate directly from acidic water.

[35] Interestingly, the concretions observed in bedrock became notably smaller and somewhat more irregular in shape after Opportunity moved southward from Endurance crater. This trend first became apparent in Microscopic Imager images acquired at Vostok crater, and has continued with increasing distance to the south. MOLA topographic data suggest that the terrain rises gently to the south, so if the beds are horizontal then a southward traverse may have taken the rover into stratigraphically higher units where concretion formation has been less prevalent.

[36] A second important class of diagenetic features found within outcrop rock consists of small elongate voids [*Herkenhoff et al.*, 2004] that are distributed abundantly but heterogeneously at both Eagle and Endurance craters. These features, up to $\sim$1 cm long and 1–2 mm wide where they intersect the rock surface, exhibit distinctive lozenge or tabular shapes and are dispersed through the rock at random orientations. The voids have been interpreted as crystal molds formed by the dissolution of highly soluble minerals [*Squyres et al.*, 2004b; *Herkenhoff et al.*, 2004], probably of monoclinic habit. The molds may have resulted from dissolution of some late-forming evaporitic mineral, perhaps melanterite (a hydrated ferrous sulfate) or Mg-, Fe-, or Ca-chlorides [*McLennan et al.*, 2005].

[37] Unlike the ubiquitous concretions, crystal molds and other secondary porosity in the rocks are not distributed evenly through the section. They are found in abundance in beds exposed at Eagle crater and in the apparently correlative upper portions of the section at Endurance crater. They are less prevalent, however, in deeper portions of the section where recrystallization has been most pronounced.

[38] Outcrop rocks also include two or more generations of cement [*McLennan et al.*, 2005]. These include both early pore-filling cements that are related to the original lithification of the sediments, and later cements formed by recrystallization. The latter are best developed around spherules, where they cement sulfate-rich sand grains together or completely recrystallize surrounding sediment to form distinctive spherule overgrowths. When subjected to erosion, the tightly cemented and resistant materials around spherules can form small pedestals or sockets [*Herkenhoff et al.*, 2004]. Cement mineralogy is not well constrained in either instance, but likely candidates include Mg-, Ca-, and Fe-sulfates (including jarosite), chlorides, hematite, and amorphous silica [*McLennan et al.*, 2005].

[39] The distribution of cements is also discontinuous throughout the section. As noted above, secondary cementation/recrystallization is pervasive in the lower portion of the section, in some strata to the point that the primary stratification is no longer evident. While some cements in

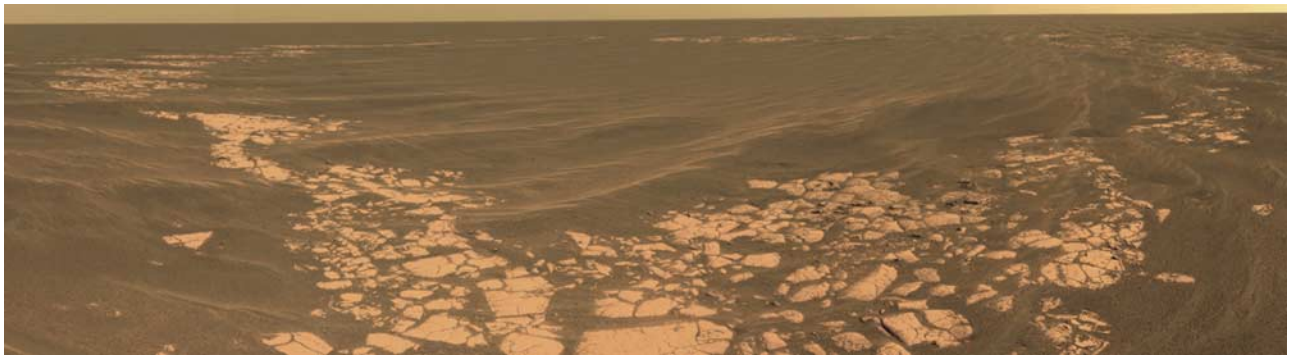

Figure 10. Approximate true color Pancam panorama of Vostok crater. Image acquired on Sol 400.

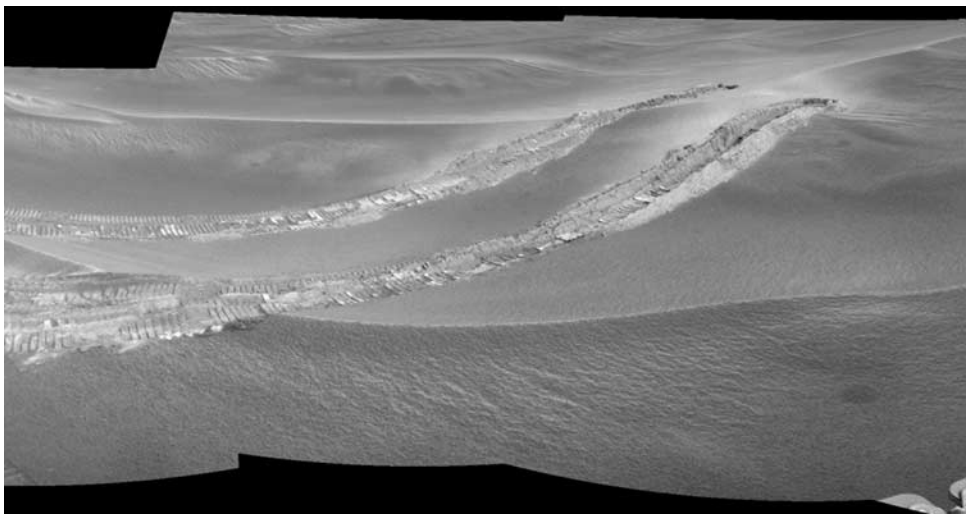

Figure 11. Navcam panorama of Purgatory Ripple. Image acquired on Sol 494.

the lower portion of the section clearly began as overgrowths around spherules, others form spherule-free nodules that apparently developed around other nucleation sites.

[40] The precipitation and recrystallization of cements, the formation and subsequent dissolution of the apparent monoclinic crystals now recorded as molds, the formation of the hematitic concretions, and the precipitation of second-generation cements around spherule surfaces all speak to a complex history of early diagenesis mediated by groundwater flow [*McLennan et al.*, 2005]. In contrast, diagenesis postdating the Endurance crater impact appears to have been limited.

4.2. Soils

[41] Inferences for the origin and evolution of soils examined by Opportunity are derived from remote sensing of the materials in Eagle and Endurance craters, remote sensing of the eolian ripples that dominate the plains landscape (Figure 12), and MI, Mössbauer, and APXS measurements of natural and disturbed soils [*Arvidson et al.*, 2004; *Christensen et al.*, 2004; *Soderblom et al.*, 2004; *Sullivan et al.*, 2005; *Yen et al.*, 2005; *Weitz et al.*, 2006]. The disturbed soil measurements were performed on four trenches (Table 4) and several other areas disturbed by the rover's wheels during driving.

4.2.1. Geochemistry and Mineralogy

[42] The soils at Meridiani are not primarily derived from the sulfate-rich outcrop rocks. Instead, they are dominated by olivine-bearing basalt and, near the surface, hematite-rich concretions and concretion fragments [*Klingelhöfer et al.*, 2004; *Soderblom et al.*, 2004; *Yen et al.*, 2005; *Weitz et al.*, 2006]. Soil composition varies across the eolian ripples. The crests of ripples are covered with a dense monolayer of sand to granule sized concretions and concretion fragments. Ripple trough surfaces, in contrast, are dominated by basaltic sands and nanophase iron oxides, and have lower concentrations of concretions and concretion fragments.

[43] Below the surface, bulk plains soils exposed by trenching show evidence for basaltic composition, including olivine, pyroxene, plagioclase feldspar, nanophase iron oxides and magnetite. Concretions and concretion fragments are rare, and sulfates are effectively absent.

4.2.2. Physical Properties

[44] In general, the concretions and concretion fragments found in plains soils in the vicinity of Eagle and Endurance craters are smaller than those observed within nearby bedrock, presumably reflecting the greater erosion that the loose concretions and fragments on the plains have suffered. They are also generally smaller on ripple crests than they are between ripples. There is a trend to smaller hematite-rich granules in the soils as Opportunity drove southward [*Weitz et al.*, 2006], perhaps reflecting the generally smaller sizes of the concretions in the local source rock.

[45] Examination of trenches excavated using the rover's wheels, as well as areas disturbed by the wheels during normal driving, provides insight into the cohesive properties of soils. The imprint of the Mössbauer Spectrometer contact plate, which is typically pressed into soils with a preload of $\sim$1 N, provides an additional perspective. The very surface of the disturbed soils on the plains typically exhibits a platy or cloddy reddish appearance consistent with a slight degree of induration (Figure 13). Microscopic Imager views of the very detailed molds produced by the Mössbauer Spectrometer contact plate suggest that the bulk soils beneath the surface are poorly sorted sands in which silt to dust-sized particles are able to fill in the pores and thus provide a modest degree of cohesion that maintains molded shapes. This is particularly true of the materials encountered as Opportunity traversed south, including the exquisite molds produced in disturbed soils within Purgatory Ripple (Figure 11). In fact, orbital data suggest a greater contribution of dust in ripples for this region as opposed to the plains in the vicinity of Endurance [*Arvidson et al.*, 2006b].

4.2.3. Soil-Atmosphere Interactions

[46] Wind has strongly influenced soil at Meridiani Planum. While some eolian mobilization of finer particles currently occurs, much of the eolian geomorphology of the plains records a previous climate regime with somewhat different wind patterns than at present. Opportunity's discovery of fields of eolian ripples extending to all

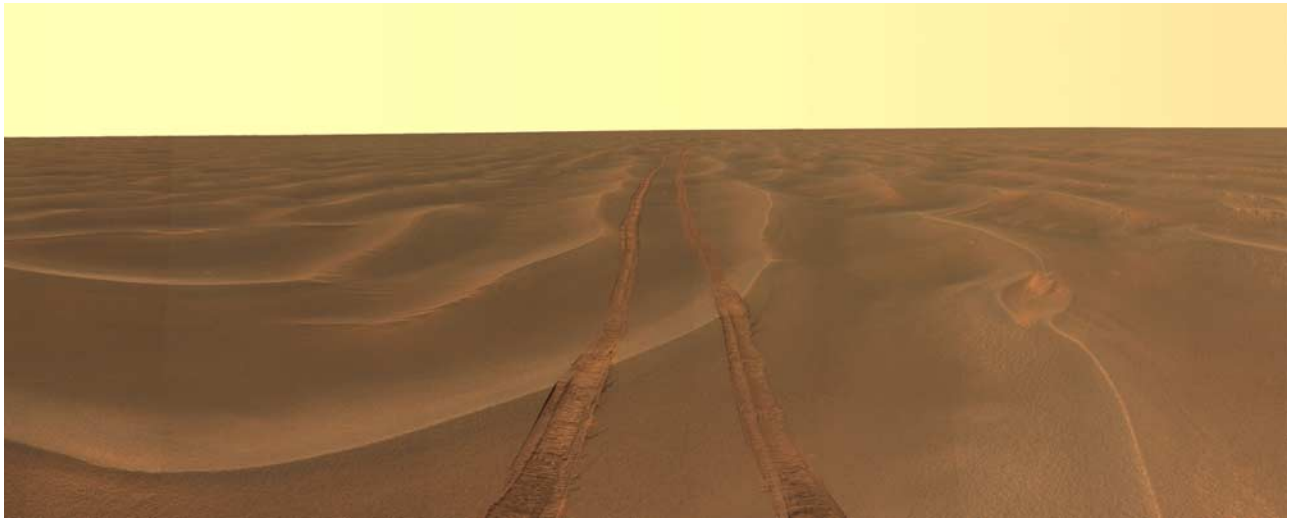

Figure 12. Approximate true color Pancam panorama of eolian ripples on the Meridiani plains. Image acquired on Sols 456 to 464; part of the "Rub Al Khali" panorama acquired from Purgatory Ripple.

horizons on the plains was unanticipated. These ripples, composed of 1–2 mm hematitic grains mixed with much finer basaltic particles, are more stable than much smaller ripples found in isolated saltation traps (e.g., crater floors) that are composed almost exclusively of ~100 μm basaltic sand. Evidence for saltation of ~100 μm particles was a surprise compared with previous, long-standing predictions that saltation particle sizes would be several factors larger.

[47] Deposits of dust-sized particles were suggested by orbital images showing bright wind streaks extending SE from many craters in the landing area. The current level of wind-related mobility of soil particles was investigated by Opportunity where settings and circumstances allowed. The bright wind streak extending SE from the rim of Eagle crater was briefly examined immediately after Opportunity left the crater. The presence of air fall dust found within the streak is responsible for its appearance from orbit [*Sullivan et al.*, 2005], consistent with models for bright streak formation involving discontinuous patches of air fall dust remaining in wind shadows behind obstacles [*Veverka et al.*, 1981; *Thomas et al.*, 1984]. Near the landing site, in places where a longer record of repeated orbital image coverage exists, some bright streaks were observed to reverse direction on timescales related to recent dust storms, implying wind streaks such as those extending from Eagle and Endurance craters are transient and active in the current climate [*Sullivan et al.*, 2005; *Jerolmack et al.*, 2006].

[48] Small ripples composed of ~100 μm basaltic sand on the floor of Eagle crater have orientations consistent with the same formative NW winds as the bright wind streaks, implying these basaltic ripples, too, are mobilized in the current climate. Significantly, however, the extensive fields of larger, mixed-grain ripples that cover the plains are misaligned with such winds, indicating that wind in the current wind regime has not been strong enough to overcome observed induration of their surfaces and mobilize these bedforms [*Sullivan et al.*, 2005]. These ripples are oriented SSW-NNE; partially reoriented bedforms in some areas have alignments intermediate between the original orientations and those of the more recently active basaltic sand ripples in Eagle crater. Altogether, a clockwise rotation of strong, formative (likely reversing) wind directions of about 40 degrees is implied between the last major movements of the larger plains ripples, and the current formative wind directions influencing free basaltic sand at the surface and bright wind streak formation [*Sullivan et al.*, 2005]. Current eolian activity seems restricted to winds moving a

Figure 13. False color Pancam image of disturbed soil near Purgatory Ripple. Reddish indurated clods on the left side of the image have been created by rover wheel interactions with the soil. The partial circular impression near the center of the image was created by the Mössbauer Spectrometer contact plate. Image acquired on Sol 510 using Pancam's 753 nm, 535 nm, and 432 nm filters, L2, L5, and L7.

sparsely distributed population of ~100 μm basaltic sand out on the plains (collecting temporarily in traps), and erasing air fall-refreshed dust deposits.

4.3. Loose Rocks on the Plains

[49] In addition to outcrop rock and soils, Opportunity has also observed several loose rocks on the plains. The two most noteworthy of these are Bounce Rock and Heat Shield Rock.

[50] Bounce Rock [*Squyres et al.*, 2004a] was encountered about 20 m beyond the rim of Eagle crater. The composition of Bounce Rock is unique among all materials observed to date by either rover. Its Mössbauer spectrum is dominated entirely by pyroxene, with no other Fe-bearing minerals present in detectable quantities [*Klingelhöfer et al.*, 2004]. The APXS chemistry is basaltic, with a normative mineralogy dominated by pyroxene and lacking in olivine [*Rieder et al.*, 2004]. In both its mineralogy and chemistry, Bounce Rock is notably similar to Lithology B of the shergottite meteorite EETA79001. The distinct characteristics of Bounce Rock, together with its isolated occurrence, suggest that it may not be locally derived. We have suggested that it may have been ejected from a relatively fresh, 25-km crater located 75 km to the southwest whose continuous ejecta lies atop the Meridiani plains [*Squyres et al.*, 2004a].

[51] Heat Shield Rock was found just several meters from Opportunity's heat shield. It was first identified as an interesting target on the basis of its unusual appearance in Pancam images (Figure 9), which show a highly pitted surface that is gray in tone with quasi-specular highlights. The first indication of a metallic composition came when Mini-TES spectra suggested a thermal emissivity of ~0.35. A metallic composition was confirmed with Mössbauer and APXS data. The Mössbauer spectrum of Heat Shield Rock is dominated by kamacite, an iron-nickel alloy common in metallic meteorites. APXS data showed a composition dominated by Fe, with about 7% Ni and trace amounts of Ge and Ga, consistent with Heat Shield Rock being a type IAB iron meteorite. Because of this composition and the inferred hardness of Heat Shield Rock, no attempt was made to abrade it with the RAT.

[52] A ~3 cm rock fragment named Barberton was investigated on Sols 121 and 122 along the rim of Endurance crater. Barberton was too small to be brushed or abraded with the RAT. APXS data reveal a composition rich in Mg and Ni and poor in Al and Ca, unlike any other material analyzed by Opportunity. The Fe-bearing mineralogy shown by Barberton's Mössbauer spectrum is dominated by olivine and contains kamacite, also suggesting a meteoritic origin for this rock

[53] Some other small loose rocks on the plains, for example Russet, which was investigated on Sols 380–381, are sulfate-rich rocks clearly derived from Meridiani outcrops, and may represent distal fragments of impact crater ejecta.

5. Ancient Environmental Conditions at Meridiani Planum

[54] All of the outcrop rocks examined to date at Meridiani Planum are sandstones. The sand grains that form them are dominated by a mixture of fine-grained altered siliciclastic phases and sulfate salts. This is true even for the lower unit of the Burns formation, which was not studied in situ but which has the same sulfate-rich Mini-TES spectral properties as the rest of the sequence. Accordingly, we interpret the entire Burns formation as owing its origin to the reworking of mixed sulfate-silicate sediments. The initial materials formed by chemical weathering of olivine basalt in aqueous solutions of sulfuric acid, forming sulfate (and perhaps minor other) salts that accumulated with fine grained silicates. Subsequent erosion and redeposition of these materials as sand grains formed the beds observed in outcrop [*Squyres et al.*, 2004b].

[55] Because all outcrop rocks observed by Opportunity to date have been reworked by wind and water, none of them reveal the environment in which the sulfate-rich sand grains originally formed. Given the compelling evidence for emergence of groundwaters at Meridiani under generally arid climate conditions, we suggest that the most likely mechanism is that grains originated by erosion from a "dirty playa," a pan of sulfate precipitates and fine-grained siliciclastic particles formed by interaction of precursor basalts with acidic groundwaters, followed by evaporation. Whatever the formation mechanism, however, it is clear that the grains now observed in outcrop were emplaced by eolian and aqueous processes, and that after their emplacement they interacted with substantial quantities of groundwater.

[56] The reworking of outcrop rocks also prevents us from pinpointing the location where the sand grains formed. We note, however, that there is no need to invoke transport to Meridiani from a distant source region. The eolian and aqueous processes that produced the observed sedimentary facies could have operated exclusively on local scales, so it is plausible that the sulfate-rich sand grains formed at Meridiani, rather than having been transported from elsewhere.

[57] The style of reworking of the sand grains in the Burns formation varies within the sequence in a way that suggests the influence of a fluctuating water table [*Grotzinger et al.*, 2005]. The lower unit represents an eolian dune environment, overlain by sand sheet deposits that may have formed along dune margins and have been transitional to the water-lain deposits in the upper part of the upper unit. Clearly the lower unit was deposited under arid conditions. However, the irregular, scoured nature of the contact between the lower and middle units led us [*Grotzinger et al.*, 2005] to propose that the lower unit may have been moist or already lightly cemented by the time of the scouring, providing evidence for a rise in the water table after dune formation. The presence of sand sheet deposits above this contact suggests that while the surface may have become damp, it was not yet flooded. However, by the time the water-lain upper part of the upper unit had formed, the water table had risen to and intersected the surface. Fluctuations in water table levels could have been accomplished by changes in the flux of groundwater, changes in sediment supply, or a combination of the two.

[58] The diagenetic history of the rocks at Meridiani also provides evidence for water table fluctuations. As already noted, the contact between the middle and upper units at Burns Cliff is diagenetic in nature, indicating that groundwater rose to but not above that level for some period of time. In fact, *McLennan et al.* [2005] cite evidence for at least four separate episodes of groundwater influx. The first, of course, involves the water that produced the grains that

comprise all of the materials present. A second episode may have wetted and lightly cemented the lower unit prior to formation of the scoured contact between the lower and middle units. The third influx culminated in the rise of water to the surface and the development of the subaqueous current ripples in the upper part of the upper unit. This same episode may have led to much of the observed cementation throughout the sequence. A fourth influx resulted in precipitation of the hematite-rich concretions found throughout the Burns formation.

[59] In summary, we interpret the Burns formation to be sedimentary rocks formed in a wind-swept, arid surface environment with a fluctuating water table. Water rose occasionally to the surface, and sulfate-rich sand grains were reworked by the wind to form dunes and sand sheets. The rocks observed by Opportunity to date record a transition from dunes to dune-marginal sand sheets to transient surface water. Multiple introductions of groundwater governed diagenesis, including the formation of the ubiquitous hematite-rich "blueberries."

[60] Key characteristics of the Burns formation constrain interpretations of the environmental conditions under which it formed. The unit is dominated by eolian sands, indicating that surface conditions were generally arid. The mineralogy, particularly the presence of jarosite, indicates that ambient waters were acidic. And the oxidation state of iron, with most present as Fe^{3+} even though the unweathered source material was Fe^{2+} in basalt, indicates that conditions were oxidizing. The occurrence and preservation of highly soluble sulfate salts, such as Mg-sulfates, further suggests that water was persistently at high ionic strength. So despite the abundance of water when the rocks at Meridiani formed, arid, high ionic strength, acidic and oxidizing conditions prevailed and would have posed multiple challenges for life [*Knoll et al.*, 2005].

References

Arvidson, R. E., S. W. Squyres, E. T. Baumgartner, P. S. Schenker, C. S. Niebur, K. W. Larsen, F. P. Seelos IV, N. O. Snider, and B. L. Jolliff (2002), FIDO prototype Mars rover field trials, Black Rock Summit, Nevada, as test of the ability of robotic mobility systems to conduct field science, *J. Geophys. Res.*, *107*(E11), 8002, doi:10.1029/2000JE001464.

Arvidson, R. E., et al. (2004), Localization and physical property experiments conducted by Opportunity at Meridiani Planum, *Science*, *306*, 1730–1733.

Arvidson, R. E., et al. (2006a), Overview of the Spirit Mars Exploration Rover Mission to Gusev Crater: Landing site to Backstay Rock in the Columbia Hills, *J. Geophys. Res.*, *111*, E02S01, doi:10.1029/2005JE002499.

Arvidson, R. E., et al. (2006b), Nature and origin of the hematite-bearing plains of Terra Meridiani based on analyses of orbital and Mars Exploration rover data sets, *J. Geophys. Res.*, *111*, E12S08, doi:10.1029/2006JE002728.

Bell, J. F., III, et al. (2004), Pancam multispectral imaging results from the Opportunity rover at Meridiani Planum, *Science*, *306*, 1703–1709.

Bell, J. F., III, D. Savransky, and M. J. Wolff (2006), Chromaticity of the Martian sky as observed by the Mars Exploration Rover Pancam instruments, *J. Geophys. Res.*, *111*, E12S05, doi:10.1029/2006JE002687.

Burns, R. G. (1986), Terrestrial analogs of the surface rocks of Mars, *Nature*, *320*, 55–56.

Burns, R. G. (1987), Ferric sulfates on Mars, *Proc. Lunar Planet. Sci. Conf. 17th*, Part 2, *J. Geophys. Res.*, *92*, suppl., E570–E574.

Christensen, P. R., et al. (2000), Detection of crystalline hematite mineralization on Mars by the Thermal Emission Spectrometer: Evidence for near-surface water, *J. Geophys. Res.*, *105*(E4), 9623–9642.

Christensen, P. R., R. V. Morris, M. D. Lane, J. L. Bandfield, and M. C. Malin (2001), Global mapping of Martian hematite mineral deposits: Remnants of water-driven processes on early Mars, *J. Geophys. Res.*, *106*(E10), 23,873–23,886.

Christensen, P. R., et al. (2004), Mineralogy at Meridiani Planum from the Mini-TES experiment on the Opportunity rover, *Science*, *306*, 1733–1739.

Clark, B. C., et al. (2005), Chemistry and mineralogy of outcrops at Meridiani Planum, *Earth Planet. Sci. Lett.*, *240*, 73–94.

Fergason, R. L., P. R. Christensen, J. F. Bell III, M. P. Golombek, K. E. Herkenhoff, and H. H. Kieffer (2006), Physical properties of the Mars Exploration Rover landing sites as inferred from Mini-TES derived thermal inertia, *J. Geophys. Res.*, *111*, E02S21, doi:10.1029/2005JE002583.

Fernandez-Remolar, D. C., R. V. Morris, J. E. Gruener, R. Amils, and A. H. Knoll (2005), The Rio Tinto basin: Mineralogy, sedimentary geobiology, and implications for interpretation of outcrop rocks at Meridiani Planum, *Earth Planet. Sci. Lett.*, *240*, 149–167.

Glotch, T. D., and J. L. Bandfield (2006), Determination and interpretation of surface and atmospheric Miniature Thermal Emission Spectrometer spectral end-members at the Meridiani Planum landing site, *J. Geophys. Res.*, *111*, E12S06, doi:10.1029/2005JE002671.

Glotch, T. D., R. V. Morris, P. R. Christensen, and T. G. Sharp (2004), Effect of precursor mineralogy on the thermal infrared emission spectra of hematite: Application to Martian hematite mineralization, *J. Geophys. Res.*, *109*, E07003, doi:10.1029/2003JE002224.

Glotch, T. D., P. R. Christensen, and T. G. Sharp (2006a), Fresnel modeling of hematite crystal surfaces and application to Martian hematite spherules, *Icarus*, *181*, 408–418.

Glotch, T. D., J. L. Bandfield, P. R. Christensen, W. M. Calvin, S. M. McLennan, B. C. Clark, A. D. Rogers, and S. W. Squyres (2006b), Mineralogy of the light-toned outcrop at Meridiani Planum as seen by the Miniature Thermal Emission Spectrometer and implications for its formation, *J. Geophys. Res.*, *111*, E12S03, doi:10.1029/2005JE002672.

Golombek, M. P., et al. (2003), Selection of the Mars Exploration Rover landing sites, *J. Geophys. Res.*, *108*(E12), 8072, doi:10.1029/2003JE002074.

Golombek, M. P., et al. (2006), Erosion rates at the Mars Exploration Rover landing sites and long-term climate change on Mars, *J. Geophys. Res.*, *111*, E12S10, doi:10.1029/2006JE002754.

Grant, J. A., et al. (2006), Crater gradation in Gusev crater and Meridiani Planum, Mars, *J. Geophys. Res.*, *111*, E02S08, doi:10.1029/2005JE002465.

Greeley, R., et al. (2006), Active dust devils in Gusev crater, Mars: Observations from the Mars Exploration Rover Spirit, *J. Geophys. Res.*, *111*, E12S09, doi:10.1029/2006JE002743.

Grotzinger, J. P., et al. (2005), Stratigraphy, sedimentology and depositional environment of the Burns formation, Meridiani Planum, Mars, *Earth Planet. Sci. Lett.*, *240*, 11–72.

Herkenhoff, K. E., et al. (2004), Evidence from Opportunity's Microscopic Imager for water on Meridiani Planum, *Science*, *306*, 1723–1726.

Hurowitz, J. A., S. M. McLennan, H. Y. McSween Jr., P. A. DeSouza Jr., and G. Klingelhöfer (2006), Mixing relationships and the effects of secondary alteration in the Wishstone and Watchtower Classes of Husband Hill, Gusev Crater, Mars, *J. Geophys. Res.*, doi:10.1029/2006JE002795, in press.

Jerolmack, D. J., D. Mohrig, J. P. Grotzinger, D. A. Fike, and W. A. Watters (2006), Spatial grain size sorting in eolian ripples and estimation of wind conditions on planetary surfaces: Application to Meridiani Planum, Mars, *J. Geophys. Res.*, *111*, E12S02, doi:10.1029/2005JE002544.

Johnson, J. R., et al. (2006a), Radiative transfer modeling of dust-coated Pancam calibration target materials: Laboratory visible/near-infrared spectrogoniometry, *J. Geophys. Res.*, *111*, E12S07, doi:10.1029/2005JE002658.

Johnson, J. R., et al. (2006b), Spectrophotometric properties of materials observed by Pancam on the Mars Exploration Rovers: 2. Oppurtunity, *J. Geophys. Res.*, doi:10.1029/2006JE002762, in press.

Klingelhöfer, G., et al. (2004), Jarosite and hematite at Meridiani Planum from Opportunity's Mössbauer spectrometer, *Science*, *306*, 1740–1745.

Knoll, A. H., et al. (2005), An astrobiological perspective on Meridiani Planum, *Earth Planet. Sci. Lett.*, *240*, 179–189.

Madden, M. E. E., R. J. Bodnar, and J. D. Rimstidt (2004), Jarosite as an indicator of water-limited chemical weathering on Mars, *Nature*, *431*, 821–823.

McLennan, S. M., et al. (2005), Provenance and diagenesis of the Burns formation, Meridiani Planum, Mars, *Earth Planet. Sci. Lett.*, *240*, 95–121.

McSween, H. Y., et al. (2006), Alkaline volcanic rocks from the Columbia Hills, Gusev crater, Mars, *J. Geophys. Res.*, *111*, E09S91, doi:10.1029/2006JE002698.

Morris, R. V., et al. (2006), Mössbauer mineralogy of rock, soil, and dust at Meridiani Planum, Mars: Opportunity's journey across sulfate-rich outcrop, basaltic sand and dust, and hematite lag deposits, *J. Geophys. Res.*, doi:10.1029/2006JE002791, in press.

Rieder, R., et al. (2004), Chemistry of rocks and soils at Meridiani Planum from the Alpha Particle X-ray Spectrometer, *Science*, *306*, 1746–1749.

Ruff, S. W., P. R. Christensen, D. L. Blaney, W. H. Farrand, J. R. Johnson, J. R. Michalski, J. E. Moersch, S. P. Wright, and S. W. Squyres (2006), The rocks of Gusev Crater as viewed by the Mini-TES instrument, *J. Geophys. Res.*, doi:10.1029/2006JE002747, in press.

Smith, M. D., M. J. Wolf, N. Spanovich, A. Ghosh, D. Banfield, P. R. Christensen, G. A. Landis, and S. W. Squyres (2006), One Martian year of atmospheric observations using MER Mini-TES, *J. Geophys. Res.*, doi:10.1029/2006JE002770, in press.

Soderblom, L. A., et al. (2004), Soils of Eagle crater and Meridiani Planum at the Opportunity rover landing site, *Science*, *306*, 1723–1726.

Squyres, S. W., et al. (2003), Athena Mars rover science investigation, *J. Geophys. Res.*, *108*(E12), 8062, doi:10.1029/2003JE002121.

Squyres, S. W., et al. (2004a), The Opportunity Rover's Athena Science Investigation at Meridiani Planum, Mars, *Science*, *306*, 1698–1703.

Squyres, S. W., et al. (2004b), In situ evidence for an ancient aqueous environment at Meridiani Planum, Mars, *Science*, *306*, 1731–1733.

Sullivan, R., et al. (2005), Aeolian processes at the Mars Exploration Rover Meridiani Planum landing site, *Nature*, *436*, 58–61.

Thomas, P., J. Veverka, D. Gineris, and L. Wong (1984), "Dust" streaks on Mars, *Icarus*, *60*, 161–179.

Tosca, N. J., S. M. McLennan, B. C. Clark, J. P. Grotzinger, J. A. Hurowitz, A. H. Knoll, C. Schröder, and S. W. Squyres (2005), Geochemical modeling of evaporation processes on Mars: Insight from the sedimentary record at Meridiani Planum, *Earth Planet. Sci. Lett.*, *240*, 122–148.

Veverka, J., P. Gierasch, and P. Thomas (1981), Wind streaks on Mars: Meteorological control of occurrence and mode of formation, *Icarus*, *45*, 154–166.

Weitz, C. M., R. C. Anderson, J. F. Bell III, W. H. Farrand, K. E. Herkenhoff, J. R. Johnson, B. L. Jolliff, R. V. Morris, S. W. Squyres, and R. J. Sullivan (2006), Soil grain analyses at Meridiani Planum, Mars, *J. Geophys. Res.*, *111*, E12S04, doi:10.1029/2005JE002541.

Wolff, M. J., et al. (2006), Constraints on dust aerosols from the Mars Exploration Rovers using MGS overflights and Mini-TES, *J. Geophys. Res.*, doi:10.1029/2006JE002786, in press.

Yen, A. S., et al. (2005), An integrated view of the chemistry and mineralogy of Martian soils, *Nature*, *436*, 49–54.

Yen, A. S., et al. (2006), Nickel on Mars: Constraints on meteoritic material at the surface, *J. Geophys. Res.*, doi:10.1029/2006JE002797, in press.

R. E. Arvidson, Department Earth and Planetary Sciences, Washington University, St. Louis, MO 63130, USA.

J. F. Bell III, D. Bollen, S. W. Squyres, and R. Sullivan, Department of Astronomy, Cornell University, 428 Space Sciences Building, Ithaca, NY 14853, USA. (squyres@astrosun.tn.cornell.edu)

J. Brückner, R. Rieder, and H. Wänke, Max Planck Institut für Chemie, Kosmochemie, D-55020 Mainz, Germany.

N. A. Cabrol, NASA Ames/SETI Institute, Moffett Field, CA 94035, USA.

W. M. Calvin, Department of Geological Sciences, University of Nevada, Reno, Reno, NV 89557, USA.

M. H. Carr, U.S. Geological Survey, Menlo Park, CA 94025, USA.

P. R. Christensen, J. Farmer, R. Greeley, and J. W. Rice Jr., Department of Geological Sciences, Arizona State University, Tempe, AZ 85287, USA.

B. C. Clark, Lockheed Martin Corporation, Littleton, CO 80127, USA.

L. Crumpler, New Mexico Museum of Natural History and Science, Albuquerque, NM 87104, USA.

D. J. Des Marais and M. Sims, NASA Ames Research Center, Moffett Field, CA 94035, USA.

C. d'Uston, Centre d'Etude Spatiale des Rayonnements, F-31028 Toulouse Cedex 4, France.

T. Economou, Enrico Fermi Institute, University of Chicago, Chicago, IL 60637, USA.

W. H. Farrand, Space Science Institute, Boulder, CO 80301, USA.

W. Folkner, T. D. Glotch, M. Golombek, T. Parker, and A. Yen, Jet Propulsion Laboratory, California Institute of Technology, Pasadena, CA 91109, USA.

R. Gellert, Department of Physics, University of Guelph, Guelph, ON, Canada N1G 2W1.

S. Gorevan, Honeybee Robotics, New York, NY 10001, USA.

J. A. Grant, Center for Earth and Planetary Studies, Smithsonian Institution, Washington, DC 20560, USA.

J. Grotzinger, Division of Geological and Planetary Sciences, California Institute of Technology, Pasadena, CA 91125, USA.

K. E. Herkenhoff, J. R. Johnson, and L. A. Soderblom, U.S. Geological Survey, Flagstaff, AZ 86001, USA.

S. Hviid, Max Planck Institut für Sonnensystemforschung, Katlenburg-Lindau, Germany.

G. Klingelhöfer and C. Schröder, Institut für Anorganische und Analytische Chemie, Johannes Gutenberg-Universität, D-55099 Mainz, Germany.

A. H. Knoll, Botanical Museum, Harvard University, Cambridge, MA 02138, USA.

G. Landis, NASA Glenn Research Center, Cleveland, OH 44135, USA.

M. Lemmon, Department of Atmospheric Sciences, Texas A&M University, College Station, TX 77843, USA.

R. Li, Department of Civil and Environmental Engineering and Geodetic Science, Ohio State University, Columbus, OH 43210, USA.

M. B. Madsen, Niels Bohr Institute, Ørsted Laboratory, DK-2100 Copenhagen, Denmark.

M. C. Malin, Malin Space Science Systems, San Diego, CA 92191, USA.

S. M. McLennan and N. J. Tosca, Department of Geosciences, State University of New York, Stony Brook, NY 11794, USA.

H. Y. McSween and J. Moersch, Department of Earth and Planetary Sciences, University of Tennessee, Knoxville, TN 37996, USA.

D. W. Ming and R. V. Morris, NASA Johnson Space Center, Houston, TX 77058, USA.

L. Richter, DLR Institute of Space Simulation, D-51170 Cologne, Germany.

M. Smith, NASA Goddard Space Flight Center, Greenbelt, MD 20771, USA.

P. Smith, Lunar and Planetary Laboratory, University of Arizona, Tucson, AZ 85721, USA.

T. Wdowiak, Department of Physics, University of Alabama at Birmingham, Birmingham, AL 35294, USA.

M. Wolff, Space Science Institute, Martinez, GA 30907, USA.